INFERENCE OF CELL TYPE COMPOSITION FROM HUMAN BRAIN TRANSCRIPTOMIC DATASETS ILLUMINATES THE EFFECTS OF AGE, MANNER OF DEATH, DISSECTION, AND PSYCHIATRIC DIAGNOSIS

*Megan Hastings Hagenauer, Ph.D.[1], Jun Z. Li, Ph.D.[2], David M. Walsh, Psy.D.[3], Marquis P. Vawter, Ph.D.[3] Robert C. Thompson, Ph.D.[1], Cortney A. Turner, Ph.D.[1], William E. Bunney, M.D.[3], Richard M. Myers, Ph.D.[4], Jack D. Barchas, M.D.[5], Alan F. Schatzberg, M.D.[6], Stanley J. Watson, M.D., Ph.D.[1], Huda Akil, Ph.D.[1]

[1]Mol. Behavioral Neurosci. Inst., Univ. of Michigan, Ann Arbor, MI, USA; [2]Genet., Univ. of Michigan, Ann Arbor, MI, USA; [3]Univ. of California, Irvine, CA; [4]HudsonAlpha Inst. for Biotech., Huntsville, AL, USA; [5]Stanford, Palo Alto, CA, [6]Cornell, New York, NY, USA

*Corresponding Author: Megan Hastings Hagenauer, Ph.D.

e-mail: hagenaue@umich.edu

Molecular Behavioral Neuroscience Institute (MBNI)

205 Zina Pitcher Pl.

Ann Arbor, MI 48109

Abstract

Most neuroscientists would agree that psychiatric illness is unlikely to arise from pathological changes that occur uniformly across all cells in a given brain region. Despite this fact, the majority of transcriptomic analyses of the human brain to date are conducted using macro-dissected tissue due to the difficulty of conducting single-cell level analyses on donated post-mortem brains. To address this issue statistically, we compiled a database of several thousand transcripts that were specifically-enriched in one of 10 primary brain cell types identified in published single cell type transcriptomic experiments. Using this database, we predicted the relative cell type composition for 157 human dorsolateral prefrontal cortex samples using Affymetrix microarray data collected by the Pritzker Neuropsychiatric Consortium, as well as for 841 samples spanning 160 brain regions included in an Agilent microarray dataset collected by the Allen Brain Atlas. These predictions were generated by averaging normalized expression levels across the transcripts specific to each primary cell type to create a "cell type index". Using this method, we determined that the expression of cell type specific transcripts identified by different experiments, methodologies, and species clustered into three main cell type groups: neurons, oligodendrocytes, and astrocytes/support cells. Overall, the principal components of variation in the data were largely explained by the neuron to glia ratio of the samples. When comparing across brain regions, we were able to statistically identify canonical cell type signatures – increased endothelial cells and vasculature in the choroid plexus, oligodendrocytes in the corpus callosum, astrocytes in the central glial substance, neurons and immature cells in the dentate gyrus, and oligodendrocytes and interneurons in the globus pallidus.

The relative balance of these cell types was influenced by a variety of demographic, pre- and post-mortem variables. Age and prolonged hypoxia around the time of death were associated with decreased neuronal content and increased astrocytic and endothelial content in the tissue, replicating the known higher vulnerability of neurons to adverse conditions and illustrating the proliferation of vasculature in a hypoxic environment. We also found that the red blood cell content was reduced in individuals who died in a manner that involved systemic blood loss. Finally, statistically accounting for cell type improved both the sensitivity and interpretability of diagnosis effects within the data. We were able to observe a decrease in astrocytic content in subjects with Major Depressive Disorder, mirroring what had been previously observed morphometrically. By including a set of “cell type indices” in a larger model examining the relationship between gene expression and neuropsychiatric illness, we were able to successfully detect almost twice as many genes with previously-identified relationships to bipolar disorder and schizophrenia than using more traditional analysis methods.

1. Introduction

The human brain is a remarkable mosaic of diverse cell types stratified into rolling cortical layers, arching white matter highways, and interlocking deep nuclei. In the past decade, we have come to recognize the importance of this cellular diversity in even the most basic neural circuits. At the same time, we have developed the capability to comprehensively measure the thousands of molecules essential for cell function. These insights have provided conflicting priorities within the study of psychiatric illness: do we carefully examine individual molecules within their cellular and anatomical context or do we dissect larger tissue samples in order to extract sufficient transcript or protein to perform full unbiased transcriptomic or proteomic analyses? In rodent models, researchers have escaped this dilemma by a boon of new technology: single cell laser capture, cell culture, and cell-sorting techniques that can provide sufficient extract for transcriptomic and proteomic analyses. However, single cell analyses of the human brain are far more challenging (1–3) – live tissue is only available in the rarest of circumstances (such as temporal lobe resection) and high quality post-mortem tissue is precious, especially tissue donated by the families of individuals with rare psychiatric or neurological disorders.

Therefore, to date, the vast majority of unbiased transcriptomic analyses of the human brain have been conducted using macro-dissected, cell-type heterogeneous tissue. They have provided us with novel hypotheses (e.g., (4,5)), but researchers who work with the data often report frustration with the relatively small number of candidate molecules that survive analyses using their painstakingly-collected samples, as well as the overwhelming challenge of interpreting molecular results in isolation from their

respective cellular context. At the core of this issue is the inability to differentiate between (1) alterations in gene expression that reflect an overall disturbance in the relative ratio of the different cell types comprising the tissue sample, and (2) intrinsic dysregulation of one or more cell types, indicating perturbed biological function.

In this manuscript, we present results from an easily accessible solution to this problem that allows researchers to statistically estimate the relative number or transcriptional activity of particular cell types in macro-dissected human brain microarray data by tracking the collective rise and fall of previously identified cell type specific transcripts. Similar techniques have been used to successfully predict cell type content in human blood samples (6–9), as well as diseased and aged brain samples (10–12). Our method was specifically designed for application to large, highly-normalized human brain transcriptional profiling datasets, such as those commonly used by neuroscientific research bodies such as the Pritzker Neuropsychiatric Research Consortium and the Allen Brain Institute.

We took advantage of a series of newly available data sources depicting the transcriptome of known cell types, and applied them to infer the relative balance of cell types in our tissue samples in a semi-supervised fashion. We draw from seven large studies detailing cell-type specific gene expression in a wide variety of cells in the forebrain and cortex (2,13–18). Our analyses include all major categories of cortical cell types (17), including two overarching categories of neurons that have been implicated in psychiatric illness (19): projection neurons, which are large, pyramidal, and predominantly excitatory, and interneurons, which are small and predominantly inhibitory (20). These are accompanied by the three prevalent forms of glia that make

up the majority of cells in the brain: oligodendrocytes, which provide the insulating myelin sheath that enhances electrical transmission in axons (21), astrocytes, which help create the blood-brain barrier and provide structural and metabolic support for neurons, including extracellular chemical and electrical homeostasis, signal propagation, and response to injury (21), and microglia, which serve as the brain's resident macrophages and provide an active immune response (21). We also incorporate structural and vascular cell types: endothelial cells, which line the interior surface of blood vessels, and mural cells (smooth muscle cells and pericytes), which regulate blood flow (22). Progenitor cells may be less prevalent in the aging human brain, but are widely regarded as important for the pathogenesis of mood disorders (23), and thus were also included in our analysis. Within the cortex, these cells mostly take the form of immature oligodendrocytes (17). Finally, the primary cells found in blood, erythrocytes or red blood cells (RBCs), carry essential oxygen throughout the brain. These cells do not contain a cell nucleus and do not generate new RNA, but still contain an existing, highly-specialized transcriptome (24). The relative presence of these cells could arguably represent overall blood flow, the functional marker of regional neural activity traditionally used in human imaging studies.

To characterize the balance of these cell types in psychiatric samples, we first compare the predictive value of cell type specific transcripts identified by diverse data sources and then summarize their collective predictions of relative cell type balance into covariates that can be used in larger linear regression models. We demonstrate that statistically estimating the relative cell type balance of samples can explain a large percentage of the variation in human brain microarray datasets. We also find that the

incorporation of a set of "cell type indices" into a larger regression model can successfully predict other cell type-enriched gene expression as well as known changes in cell type balance in response to age, aerobic environment, large scale blood loss, and dissection. Finally, we demonstrate that this method enhances our ability to discover and interpret psychiatric effects in human brain microarray datasets, uncovering known changes in cell type balance in relationship to major depressive disorder and increasing our sensitivity to detect genes with previously-identified relationships to bipolar disorder and schizophrenia.

2. Results

2.1 Compiling a Database of Cell Type Specific Transcripts

To perform this analysis, we compiled a database of several thousand transcripts that were specifically-enriched in one of nine primary brain cell types within seven published single-cell or purified cell type transcriptomic experiments for mammalian brain tissues (2,13–18) (**Suppl. Table 1**). These primary brain cell types included six types of support cells: astrocytes, endothelial cells, mural cells, microglia, immature and mature oligodendrocytes, as well as two broad categories of neurons (interneurons and projection neurons) and neurons in general. The experimental and statistical methods for determining whether a transcript was enriched in a particular cell type varied by publication (**Figure 1**), and included both RNA-Seq and microarray datasets. We focused on cell-type specific transcripts identified using cortical or forebrain samples because the data available for these brain regions was more plentiful than for the deep

93 nuclei or the cerebellum. In addition, we artificially generated a list of 17 transcripts
94 specific to erythrocytes (red blood cells or RBC) by searching Gene Card for erythrocyte
95 and hemoglobin-related genes (http://www.genecards.org/). In all, we curated gene
96 expression signatures for 10 cell types expected to account for most of the cells in the
97 brain.

98 Most of the cell-type specific transcripts were derived from microarray
99 experiments using cDNA extracted from laboratory mice, therefore in order to use this
100 information for the analysis of human microarray data it was necessary to identify the
101 respective orthologs for the cell type specific transcripts in humans using HCOP:
102 Orthology Prediction Search (http://www.genenames.org/cgi-bin/hcop). Our final
103 database included 2499 unique human-derived or orthologous transcripts, with a focus
104 on coding varieties.

Citation	Cell Origin	Method	Stringency	Derived Cortical Cell Type Indices	Transcripts/ Orthologs
Cahoy et al., *J Neuro,* 2008.	Forebrain of young transgenic mice	Fluorescent cell sorting using antibodies to deplete non-specific cell types followed by Affymetrix microarray	>20 Fold Enrichment	Astrocyte_All	73
				Neuron_All	80
				Oligodendrocyte_All	50
Zhang et al., *J Neuro* , 2014	Cortex of young transgenic mice	Fluorescent cell sorting using antibodies to deplete non-specific cell types followed by RNAseq	Top 40 transcripts with >20 Fold Enrichment	Astrocyte_All	40
				Endothelial_All	40
				Microglia_All	40
				Mural_Pericyte	40
				Neuron_All	40
				Oligodendrocyte_Myelinating	40
				Oligodendrocyte_Newly-Formed	39
				Oligodendrocyte_Progenitor Cell	40
Zeisel et al., *Science,* 2015	Somatosensory cortex and CA1 hippocampus of juvenile mice	Unbiased capture of single cells from whole tissue cell suspension followed by RNAseq	Enriched with 99.9% posterior probability	Astrocyte_All	240
				Endothelial_All	353
				Microglia_All	436
				Mural_All	155
				Neuron_Interneuron	365
				Neuron_Pyramidal_Cortical	294
				Oligodendrocyte_All	453
Darmanis et al., PNAS, 2015	Anterior temporal lobe resected from adult human epileptic patients and cortex from fetuses 16-18 wks postgestation.	Unbiased capture of single cells from whole tissue cell suspension followed by RNAseq	Top 20 enriched transcripts	Astrocyte_All	21
				Endothelial_All	21
				Microglia_All	21
				Neuron_All	21
				Oligodendrocyte_Mature	21
				Oligodendrocyte_Progenitor Cell	21
Doyle et al., *Cell,* 2008	Cortex, Striatum, Cerebellum, Spinal Cord, Basal Forebrain, and Brain Stem of young transgenic mice	Capture of translated mRNA from specific cell types labeled in transgenic mice using translating ribosome affinity purification (TRAP) followed by microarray.	Top 25 enriched transcripts determined by iterative rank comparisons	Astrocyte_All	25
				Neuron_CorticoSpinal	25
				Neuron_CorticoStriatal	25
				Neuron_CorticoThalamic	25
				Neuron_Interneuron_CORT	25
				Neuron_Neuron_CCK	25
				Neuron_Neuron_PNOC	24
				Oligodendrocyte_All	25
				Oligodendrocyte_Mature	25
Daneman et al., *PLOS,* 2010	Cortex of young transgenic mice	Fluorescent cell sorting using antibodies to deplete non-specific cell types followed by Affymetrix microarray	>20 Fold enrichment for endothelial, >8 fold enrichment for vasculature	Endothelial_All	49
				Mural_Vascular	50
Sugino et al., *Nature Neuro,* 2006	Cingulate and Somatosensory Cortices, Basolateral Amygdala, CA1-CA3 Hippocampus, and Dorsal Lateral Geniculate Nucleus of the Thalamus of transgenic mice	Hand-sorting fluorescently-labeled cells followed by amplification and Affymetrix microarray	Enriched with p< 1.5E-11	Neuron_GABA	32
				Neuron_Glutamate	67
Gene card	Human	Erythrocyte-related genes	Unknown	RBC_All	17

Figure 1. Thousands of transcripts have been identified as specifically-enriched in particular cortical cell types within published single-cell or purified cell type transcriptomic experiments. The experimental and statistical methods for determining whether a transcript was enriched in a cell type varied by publication, and included both RNA-Seq and microarray datasets.

111 ***2.2 Using Cell Type Specific Transcripts to Predict Relative Cell Content in***
112 ***Microarray Data from Macro-Dissected Human Dorsolateral Prefrontal Cortex***
113 ***Tissue***

114 Next, we examined the collective variation in the levels of cell type specific
115 transcripts in an Affymetrix microarray dataset from 157 high-quality human post-
116 mortem dorsolateral prefrontal cortex samples (**Suppl. Table 2**), including tissue from
117 subjects without a psychiatric or neurological diagnosis ("Controls", n=71), or diagnosed
118 with Major Depressive Disorder ("MDD", n=40), Bipolar Disorder ("BP", n=24), or
119 Schizophrenia ("Schiz", n= 22). The severity and duration of physiological stress at the
120 time of death was estimated by calculating an agonal factor score for each subject
121 (ranging from 0-4, with 4 representing severe physiological stress; (25,26)). Additionally,
122 we measured the pH of cerebellar tissue as an indicator of the extent of oxygen
123 deprivation experienced around the time of death (25,26) and calculated the interval
124 between the estimated time of death and the freezing of the brain tissue (the
125 postmortem interval or PMI) using coroner records.

126 To predict the relative cell content in each of the samples, we used a technique
127 validated using datasets from purified cell types and artificial cell mixtures
128 (**Supplementary Methods and Results, Suppl. Figs 1-4**). We identified 2678 gene
129 probe sets in the Affymetrix dataset that were found in our curated database of cell type
130 specific transcripts as matched by official gene symbol. We centered and scaled the
131 expression level of each gene probeset across samples (mean=0, sd=1) to prevent

132 probe sets with more variable hybridization signal from exerting disproportionate
133 influence, and then, for each sample, averaged this value across the transcripts
134 identified in each publication as specific to a particular cell type. This created 38 cell
135 type signatures derived from the cell type specific genes identified by the eight
136 publications (***"Cell Type Indices"*** **, Figure 1)**, each of which predicted the relative
137 content for one of the 10 primary cell types in our cortical samples (**Figure 2).**
138

A.

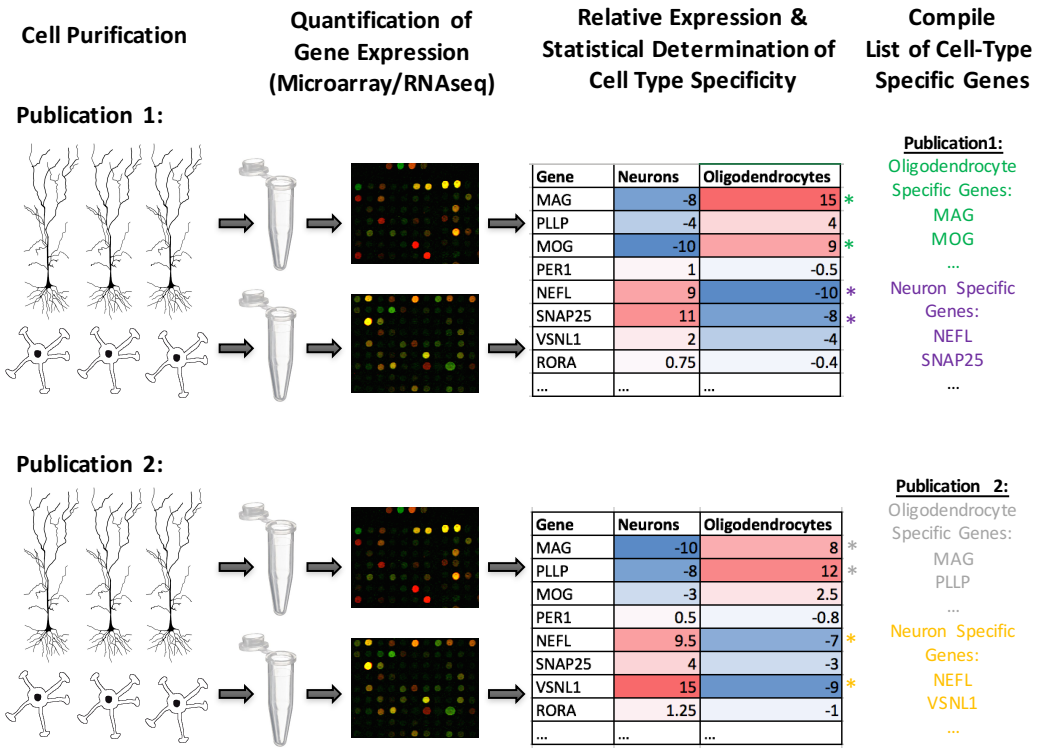

B.

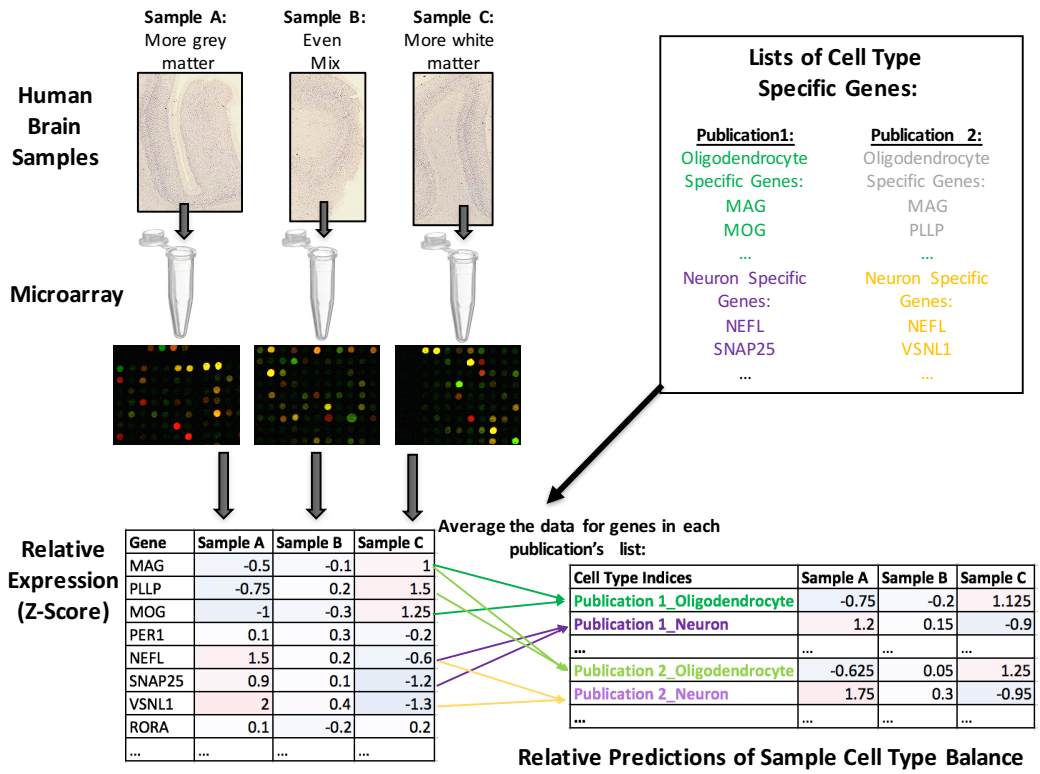

Figure 2. Predicting the relative cell type balance in human brain samples using genes previously-identified as having cell type specific expression. A. We compiled a database of genes that were identified in previous publications as specifically enriched in particular forebrain or cortical cell types. Within these publications, researchers purified particular brain cell types or individual brain cells and transcriptionally profiled them using microarray or RNA-Seq. They then performed statistical comparisons across the purified brain cell types to determine which transcripts showed relatively elevated expression in each cell type. **B.** Within the Pritzker brain tissue samples, we expected variable cell type balance that would influence the pattern of gene expression measured by microarray. To estimate this variability, we pulled out the microarray data for probe sets representing genes that had been previously identified as having cell type specific expression and then averaged

151 across the transcripts identified in each publication **(Figure 1)** as specific to a particular
152 cell type to create 38 different ***"Cell Type Indices"*** that predicted relative cell content in
153 each of the cortical samples.

154 ***2.3 There is a Strong Convergence of Cell Content Predictions Derived from Cell***
155 ***Type Specific Transcripts Originating from Different Publications***

156 We found that the predicted cell content of the prefrontal cortex samples was
157 relatively similar regardless of the origin of the cell type specific gene lists used to
158 create the predictions. When comparing the pattern of correlations between the 38 cell
159 type indices, they clearly cluster into three large umbrella categories: Neurons,
160 Oligodendrocytes, and Support Cells (Astrocytes, Microglia, and Neurovasculature*)*
161 even when the cell type signatures were derived from cell type specific gene lists from
162 different source publications, species, and methodologies. This clustering was clear
163 using visual inspection of the correlation matrix (**Figure 3)**, hierarchical clustering, or
164 consensus clustering (**Suppl. Figure 5;** ConsensusClusterPlus: (27))**.** Moreover, the
165 clustering was not due to the different publications identifying a similar subset of cell-
166 type specific genes, because the clustering persisted in a follow-up analysis in which
167 data from genes identified as cell type specific in multiple publications (e.g.,
168 Cahoy_Astrocyte and Zhang_Astrocyte) were removed list wise from the dataset
169 **(Suppl. Figure 6 & 7).** Clustering was not able to reliably discern neuronal
170 subcategories (interneurons, projection neurons) or support cell subcategories.
171 Oligodendrocyte progenitor cell indices derived from different publications did not
172 strongly correlate with each other, which may indicate a lack of significant presence of
173 progenitor cells in the cortex of our primarily middle-aged subjects.
174
175

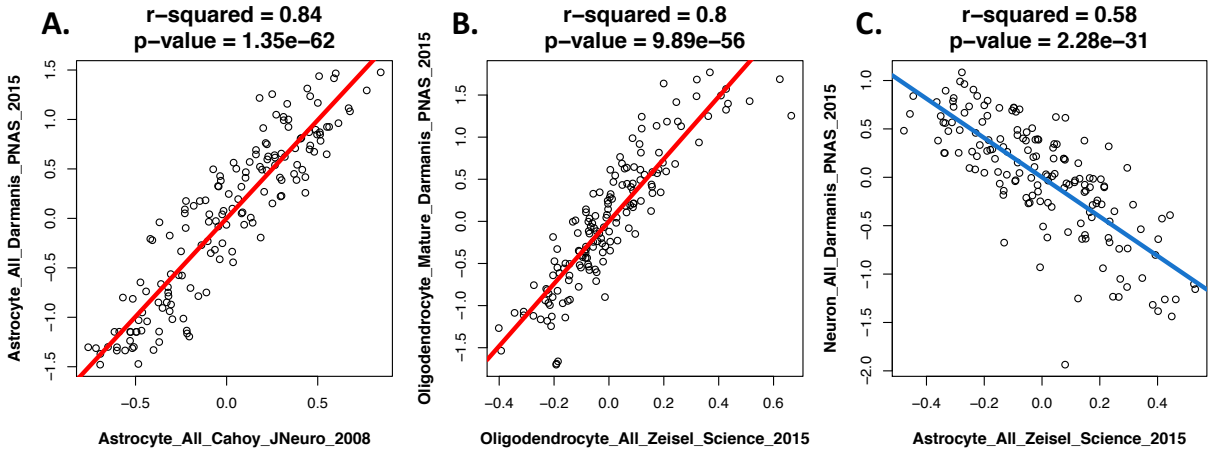
A.
r−squared = 0.84
p−value = 1.35e−62
Astrocyte_All_Darmanis_PNAS_2015
Astrocyte_All_Cahoy_JNeuro_2008
B.
r−squared = 0.8
p−value = 9.89e−56
Oligodendrocyte_Mature_Darmanis_PNAS_2015
Oligodendrocyte_All_Zeisel_Science_2015
C.
r−squared = 0.58
p−value = 2.28e−31
Neuron_All_Darmanis_PNAS_2015
Astrocyte_All_Zeisel_Science_2015

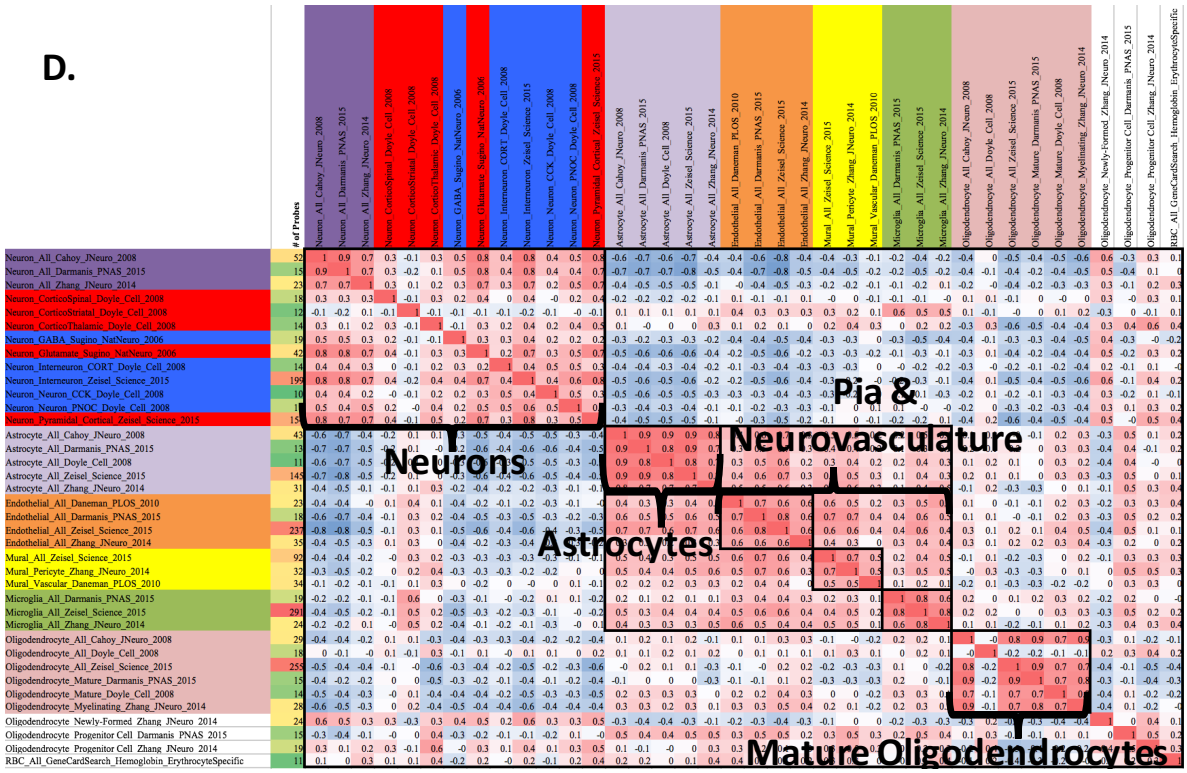
D.
Neurons
Astrocytes
Pia &
Neurovasculature
Mature Oligodendrocytes

Figure 3. There is a convergence of cell content predictions derived from cell type specific transcripts originating from different publications. A-B. There was a strong positive correlation between predictions originating from *"cell type indices"* representing the same cell type (e.g., neurons vs. neurons, oligodendrocytes vs. oligodendrocytes…) in our dorsolateral prefrontal cortical samples, even when the predictions were based on cell type specific transcripts identified by experiments using very different methodology. The examples given below include predictions based on cell type specific transcripts identified in the mouse (x-axis) vs. human (y-axis). **C.** There was a strong negative correlation between predictions originating from *"cell type indices"* representing very dissimilar cell types, such as neurons and astrocytes. **D.** The similarity of different cell type indices can be visualized using a correlation matrix. Within this matrix, correlations can range from a strong negative correlation of -1 (blue) to a strong positive correlation of 1 (red), therefore a large block of pink/red correlations is indicative of cell type indices that tend to be enriched in the same samples. The axis labels for cell type indices representing the same category of cell are color-coded: general neuronal categories are dark purple, pyramidal neurons are red, inhibitory interneurons are dark blue, astrocytes are light purple, endothelial cells are orange, mural cells are yellow, microglia are green, mature oligodendrocytes are pink, and the remaining indices remain white to represent lack of coherent categorization. The number of probes included in each index is present in the far left column (also color-coded, with green indicating few probes and red indicating many probes).

197 ***2.4 Inferred Cell Type Composition Explains a Large Percentage of the Sample-***
198 ***Sample Variability in Microarray Data from Macro-Dissected Cortical Tissue***

199 For further analyses, individual cell type indices were averaged within each of ten
200 primary categories: astrocytes, endothelial cells, mural cells, microglia, immature and
201 mature oligodendrocytes, red blood cells, interneurons, projection neurons, and indices
202 derived from neurons in general, with any transcripts that overlapped between
203 categories removed **(Suppl. Figure 8).** This led to ten consolidated primary cell-type
204 indices for each sample. Using these consolidated cell type indices and principal
205 components analysis, we found that the first principal component, which encompassed
206 23% of the variation in the full Pritzker dorsolateral prefrontal cortex microarray dataset,
207 spanned from samples with high support cell content to samples with high neuronal
208 content. Therefore, a large percentage of the variation in PC1 (91%) was accounted for
209 by an average of the astrocyte and endothelial indices ($p<2.2E-82$, with a respective r-
210 squared of 0.80 and 0.75 for each index analyzed separately) or by the general neuron
211 index ($p<6.3E-32$, r-squared=0.59; **Figure 4**). The second notable gradient in the
212 dataset (PC2) encompassed 12% of the variation overall, and spanned samples with
213 high projection neuron content to samples with high oligodendrocyte content (with a
214 respective r-squared of 0.62 and 0.42, and respective p-values of $p<8.5E-35$ and
215 $p<8.7E-20$). In general, none of the original 38 individual cell type indices were
216 noticeably superior to the indices that were averaged by primary cell type for predicting
217 the principal components of variation in the dataset, although the variation in PC1 was

218 slightly better accounted for by the general neuron index derived from ((13), r-
219 squared=0.62) and the variation in PC2 was best accounted for by the cortical
220 pyramidal neuron index (r-squared=0.65) and oligodendrocyte index (r-squared=0.57)
221 derived from (17). Human-derived indices did not outperform mouse-derived indices,
222 and indices derived from studies using stricter definitions of cell type specificity (fold
223 enrichment cut-off in **Figure 1,** *e.g.,* (13) vs. (17)) did not outperform less strict indices.
224 To investigate whether the strong relationship between the top principal
225 components of variation in our dataset and cell type composition indices originated
226 artificially due to cell type specific genes representing a large percentage of the most
227 highly variable transcripts in the dataset, we performed principal components analysis
228 after excluding all cell type specific transcripts from the dataset and still found these
229 strong correlations (**Suppl. Figure 9**). Indeed, individual cell type indices better
230 accounted for the main principal components of variation in the microarray data than all
231 other major subject variables combined (pH, Agonal Factor, PMI, Age, Gender,
232 Diagnosis, Suicide; *PC1:* R-squared=0.4272, *PC2:* R-squared=0.2176). When
233 examining the dataset as a whole, the six subject variables accounted for an average of
234 only 12% of the variation for any particular probe (R-squared, Adj.R-squared=0.0715),
235 whereas just the astrocyte and projection neuron indices alone were able to account for
236 17% (R-squared, Adj.R-squared=0.1601) and all 10 cell types accounted for an average
237 of 31% (R-squared, Adj.R-squared=0.263), almost one third of the variation present in
238 the data for any particular probe (**Suppl. Figure 10**). These results suggested that
239 accounting for cell type balance was highly important for the interpretation of microarray

data and could improve the signal-to-noise ratio in analyses aimed at identifying psychiatric risk genes.

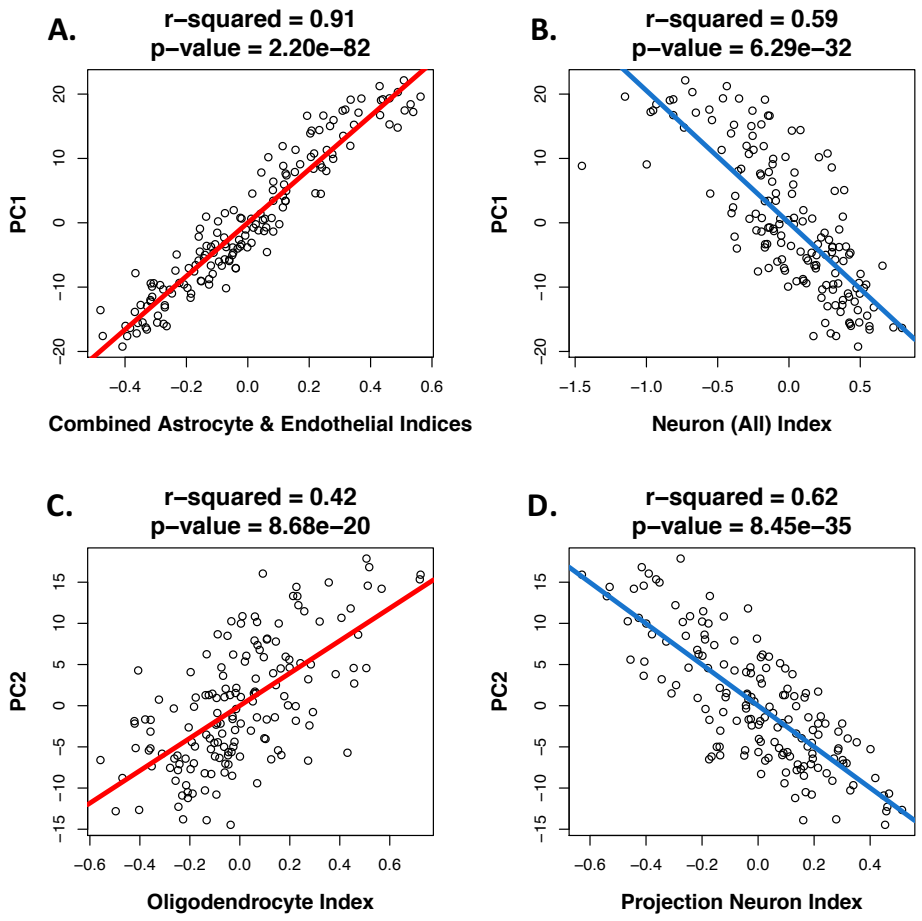

Figure 4. Cell content predictions explain a large percentage of the variability in microarray data derived from the human cortex. The first principal component of variation (PC1) encompassed 23% of the variation in the dataset, and was **A)** positively correlated with predicted "support cell" content in the samples (a combination of the astrocyte and endothelial indices: r-squared: 0.91, p<2.2E-82) and **B)** negatively correlated with predicted neuronal content (r-squared=0.59, p<6.3E-32). The second principal component of variation (PC2) encompassed 12% of variation in the dataset,

and was **C)** positively correlated with predicted oligodendrocyte content in the samples (r-squared: 0.42, p<8.7E-20) and **D)** negatively correlated with predicted projection neuron content (r-squared: 0.62, p<8.5E-35).

2.5 Cell Type Indices Predict Other Genes Known to Be Cell Type Enriched

To identify other transcripts important to cell type specific functions in the human cortex, we ran a linear model on the signal from each gene probeset in the Pritzker prefontal cortex microarray dataset that included each of the ten consolidated primary cell type indices as well as six co-variates traditionally included in the analysis of human brain gene expression data (pH, Agonal Factor, PMI, Age, Gender, Diagnosis; *Equation 1* in **Figure 5**). On average, this model explained 35% of the variation in the data (R^2). Shown in **Figure 6** are the most significant 10 gene probe sets positively associated with each cell type while controlling for the other cell types and co-variates within the model. Additional gene probe sets and statistical details can be found in **Suppl. Table 4.**

Dependent Variable: "Gene Expression" *(signal for each probe or probe set)*

	Eq.1	*Eq.3*	*Eq.4*	*Eq.5*	*Eq.6*	*Eq.7*	*Eq.8*
Variable of Interest: *Diagnosis or Psychiatric Illness*	X	X		X	X	X	X
Known Confounds: *Age, Brain pH, Agonal Factor, PMI, Gender*	X	X			X		X
The Most Prevalent Cell Types: *Astrocyte, Microglia, Oligodendrocyte, Neuron_Interneuron, Neuron_Projection*	X		X		X	X	X
Other Cell Types: *Neuron_All, Endothelial, Mural, Oligodendrocyte_Immature, RBC*	X		X				
Interaction Terms: *Variable of Interest*Cell Types*							X
Total # of Variables in the Model *(including intercept)*	17	7	11	2	12	7	17
		△ **Standard**			★★ **Best for Diagnosis Effects**		

Figure 5: Overview of the variables included in each model of gene expression (Eq.1, Eq.3-Eq.8).

General Linear Regression Model Format:

Gene Expression = β0 +β1(Variable of Interest)+β2*(Variable 2) +β3*(Variable 3)… + ε*

Astrocyte	Endothelial	Microglia	Mural	Neuron_All	Neuron_ Projection	Neuron_ Interneuron	Mature Oligodendrocyte	Red Blood Cell (RBC)
NOTCH2	**HLA-E**	**AIF1**	**TAGLN**	**VSNL1**	**PDE2A**	**TAC3**	**KLK6**	**HBD**
SDC2	**EPAS1**	**LAPTM5**	**MYL9**	**SYT1**	USF2	SLC24A3	**UGT8**	**HBB**
NTRK2	CLCN7	**IRF8**	MYH11	**SYNGR3**	DGKZ	**GAD1**	**MAG**	**PKLR**
CLDN10	**CLDN5**	**FCER1G**	CNN1	**NEFL**	**NUAK1**	**KIT**	**ELOVL1**	PGC
FGFR3	PAK4	**PTPRC**	MGP	**NRXN1**	SLC38A7	**GAD2**	**EVI2A**	*NA*
APOE	MYOF	**LAIR1**	**ACTA2**	**SNAP25**	BEGAIN	**ERBB4**	**PLLP**	DKK4
EZR	**ICAM2**	**LY86**	TP53I11	BCL2L1	KIAA0182	**LHX6**	**MOG**	LIPE
SLC1A3	ABCB1	FPR1	**COL18A1**	**MAPK1**	**KIF21B**	**SLC6A1**	**ASPA**	SPDEF
CST3	**GPR116**	**C3**	**TPM2**	EEF1A2	**PLXNA1**	**RELN**	**TF**	C19orf57
MLC1	**SDPR**	**ALOX5AP**	CRABP1	MEF2C	SLC8A2	ARL4C	**MAL**	*NA*

Figure 6. The top 10 transcripts associated with each cell type index include those previously-identified as cell type enriched in the literature. Transcripts are identified by official gene symbol. Yellow labels identify transcripts included in the original cell type index, orange transcripts were previously-identified as cell type enriched in the literature but were not included in the original list of cell type specific transcripts used to create the index. Additional transcripts and statistical details can be found in **Supplementary Table 4.**

Many of the top gene probesets that we found to be related to each of the cell type indices are already known to be associated with that cell type in previous publications, validating our methodology. Importantly, this is true even when the genes were not included in the original list of cell type specific genes used to generate the index. For example, we found that *HLA-E* (*Major Histocompatibility Complex, Class I, E*) and *EPAS1* (*endothelial PAS domain protein 1*) were both strongly associated with our endothelial index, and both are known to be involved in endothelial cell activation (*HLA-E*, in response to immune challenge: (28); *EPAS1*, in response to lack of oxygen: (29)).

286 *NOTCH2* (*Notch 2*), one of the top astrocyte-related genes, promotes astrocytic cell
287 lineage (30), and *APOE* (*Apolipoprotein E*) is primarily secreted by astrocytes in the
288 central nervous system (31). One of the top interneuron genes, *LHX6* (*LIM Homeobox*
289 *6*), is specifically enriched in parvalbumin-containing interneurons in the human cortex
290 (2). Another top interneuron gene, *ERBB4* (*Erb-B2 Receptor Tyrosine Kinase 4*),
291 controls the development of GABA circuitry in the cortex (32). The top neuron-related
292 genes include several genes related to synaptic function (*SYT1* (*Synaptotagmin I*),
293 *SYNGR3* (*Synaptogyrin 3*), *NRXN1* (*Neurexin 1*); http://www.genecards.org/). The top
294 projection neuron-related gene, *PDE2A* (*Phosphodiesterase 2A, CGMP-Stimulated*), is
295 preferentially expressed in cortical pyramidal neurons (33), and *KIF21B* (*Kinesin Family*
296 *Member 21B*) is a kinesin that has been found in the dendrites of pyramidal neurons
297 (34). We also rediscovered probesets representing genes that were listed as alternative
298 orthologs to those included in our original cell type specific gene lists (oligodendrocytes:
299 *EVI2A* vs.*CTD-2370N5.3*, microglia: *LAIR1* vs. *LAIR2*, mural cells: *COL18A1* vs.
300 *COL15A1*, *ACTA2* vs. *ACTG1*). Altogether, these results suggest that our cell type
301 indices were associated with the variability of transcripts in the cortex that represented
302 particular cell types and could re-identify known cell type specific markers.
303

304 ***2.6 Using Cell Type Specific Transcripts to Predict Cell Content in Microarray***
305 ***Data for >840 Samples from 160 Human Brain Regions***

306 For validation, we decided to also apply our cell type analysis to a large Agilent
307 microarray dataset (841 samples) spanning 160 cortical and subcortical brain regions
308 from the Allen Brain Atlas (**Suppl. Table 3;** (35)). This dataset included high-quality
309 tissue (absence of neuropathology, pH>6.7, PMI<31 hrs, RIN>5.5) from 6 human
310 subjects (36). The tissue samples were collected using a mixture of block dissection
311 and laser capture microscopy guided by adjacent tissue sections histologically stained
312 to identify traditional anatomical boundaries (37).

313 The 30,000 probes mapped onto 18,787 unique genes (as determined by gene
314 symbol). We found that 1608 of these genes were identified as having cell type specific
315 expression within our database. Then, using a procedure similar to that used for the
316 Pritzker prefrontal cortex dataset, we averaged the data from the cell-type specific
317 genes derived from each publication to predict the relative content of each of the 10
318 primary cell types in each sample.

319

320 ***2.7 Predicted Cell Content Accurately Reflects Regional Differences in Cell Type***
321 ***Balance***

322 To explore the generalizability of our method to non-cortical samples, we
323 examined the relative balance of each of the 10 primary cell types in all 160 brain
324 regions included in the Allen Brain Atlas microarray dataset. To do this, we used violin
325 plots, which are preferable for visualizing trends in data with small sample sizes (1-6

326 subjects per region). The results clearly indicated that our cell type analyses could
327 identify well-established differences in cell type balance across brain regions (**Figure 7)**.
328 Within the choroid plexus, which is a villous structure located in the ventricles made up
329 of support cells (epithelium) and an extensive capillary network (38), there is an
330 enrichment of cells related to vasculature (endothelial cells, mural cells) and immunity
331 (microglia). In the corpus callosum, which is the primary myelinated fiber tract
332 connecting the cerebral hemispheres (38), there is an enrichment of oligodendrocytes
333 and microglia. The central glial substance is enriched with glia and support cells, with a
334 particular emphasis on astrocytes. The dentate gyrus, which is one of the only
335 neurogenic regions in the adult brain (39) and which contains the predominantly
336 glutamatergic granule cells projecting into the mossy fibre pathway (40), has an
337 enrichment of both immature-like cells and projection neurons. The internal segment of
338 the globus pallidus, which is highly GABA-ergic and named after its white matter
339 intrusions (38), was enriched for oligodendrocytes, astrocytes, and microglia, as well as
340 a prominent subset of interneurons. The relative cell content predictions for the other
341 brain regions can be found in **Suppl. Table 5.** Even though this analysis was based on
342 cell type specific genes identified in the forebrain and cortex, these results provide
343 fundamental validation that each of primary consolidated cell type indices is generally
344 tracking their respective cell type in subcortical structures.
345

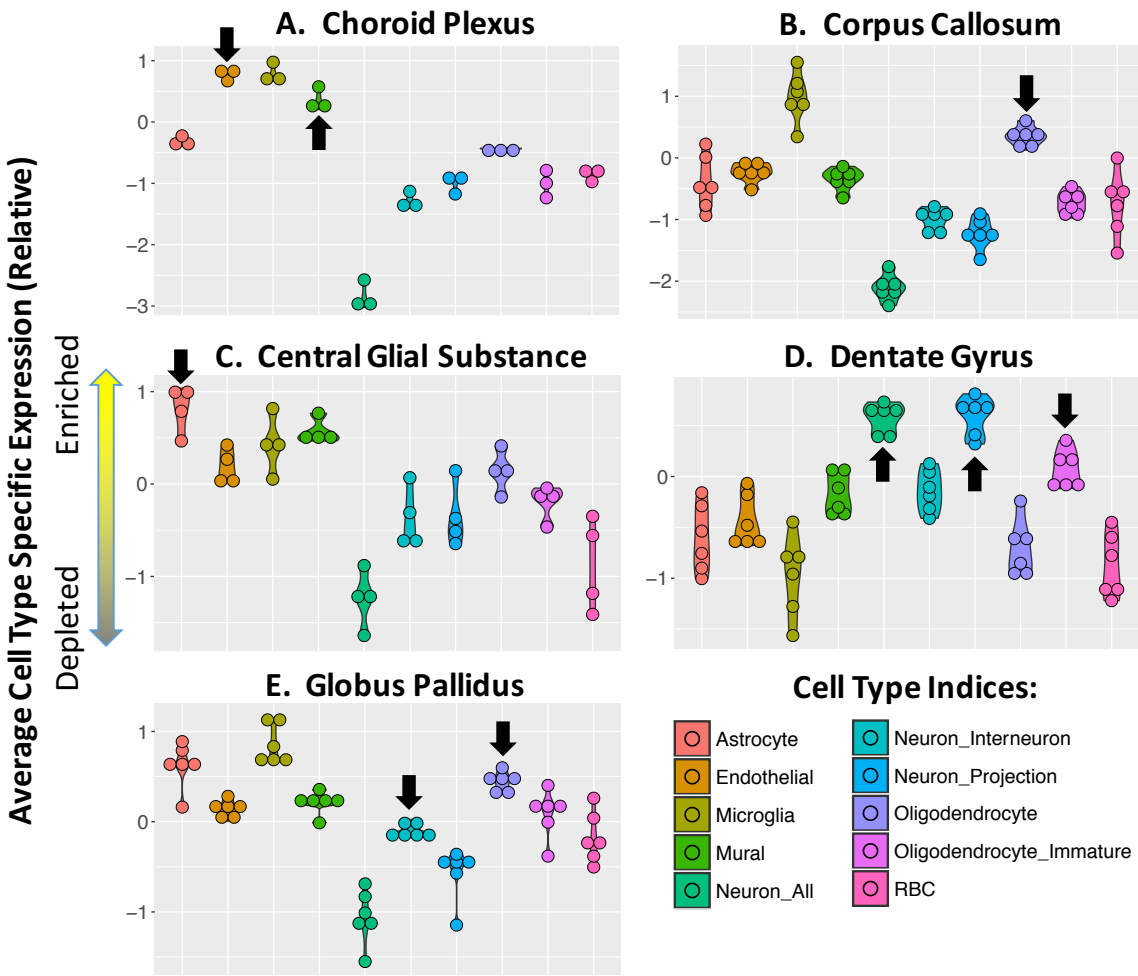

346

347 **Figure 7. Cell content predictions derived from microarray data capture canonical**
348 **regional differences in cell type balance.** As an additional form of validation, we
349 applied our cell type analysis to a large Agilent microarray dataset (841 samples)
350 spanning 160 brain regions from the Allen Brain Atlas. Depicted below is the relative
351 average cell type specific expression for each subject (dot) for each of the 10 primary
352 cell type indices. A color-coded region encompasses the data cloud for each cell type.
353 Within the example brain regions, we are able to clearly identify canonical differences in
354 cell type balance, with black arrows indicating cell types that are known to be enriched
355 in that respective region. **A.** Within the choroid plexus there is an enrichment of cells

related to vasculature (endothelial cells, mural cells) and immunity (microglia). **B.** In the corpus callosum there is an enrichment of oligodendrocytes and microglia. **C.** The central glial substance is enriched with glia and support cells, with a particular emphasis on astrocytes. **D.** The dentate gyrus has an enrichment of both immature cells and projection neurons. **E.** The internal segment of the globus pallidus was enriched for oligodendrocytes, astrocytes, and microglia, as well as a prominent subset of interneurons. The relative cell content predictions for the other brain regions can be found in **Suppl. Table 5.**

Similar to the Pritzker dataset, we outputted a table of the top genes associated with each cell type (as assessed using the model in *Equation 4*, **Figure 5**). We found that the results included a mixture of well-known cell type markers and novel findings **(Suppl. Figure 11; Suppl. Table 6)**. When this model was applied to the principal components of variation in the dataset instead of the data for individual genes, we again found that the main sources of variation in the dataset could be overwhelmingly accounted for by cell type balance (*PC1:* $F(10, 830)=1051$, $R^2=0.927$, $p<2.2e-16$; *PC2:* $F(10, 830)=96.98$, $R^2=0.539$, $p<2.2e-16$; *PC3:* $F(10, 830)=133.2$, $R^2= 0.616$, $p<2.2e-16$; *PC4:* $F(10, 830)=121.3$, $R^2= 0.594$, $p<2.2e-16$), although the specific relationships sometimes differed from what was seen in the prefrontal cortex (**Suppl. Figure 12**). Overall, these results indicate that our method for statistically predicting cell content can be a useful addition to the analysis of non-cortical as well as cortical data sets.

377 ***2.8 Cell Content Predictions Derived from Microarray Data Match Known***
378 ***Relationships Between Clinical/Biological Variables and Brain Tissue Cell***
379 ***Content***

380 We next set out to observe the relationship between the predicted cell content of
381 our samples and a variety of medically-relevant subject variables, including variables
382 that had already been demonstrated to alter cell content in the brain in other paradigms
383 or animal models. To perform this analysis, we examined the relationship between
384 seven relevant subject variables and each of the ten cell type indices in the Pritzker
385 prefrontal cortex dataset using a linear model that allowed us to simultaneously control
386 for other likely confounding variables in the dataset:
387
388 *Equation 2:*
389 $$\text{Cell Type Index} = \beta 0 + \beta 1*(\text{Brain pH}) + \beta 2*(\text{Agonal Factor})$$
390 $$+\beta 3*(\text{PMI}) + \beta 4*(\text{Age}) + \beta 5*(\text{Sex}) + \beta 6*(\text{Diagnosis}) + \beta 7*(\text{Exsanguination}) + \varepsilon$$
391

392 This analysis uncovered many well-known relationships between brain tissue cell
393 content and clinical or biological variables (**Figure 8)**. For example, we found that
394 subjects who died in a manner that involved exsanguination had a notably low red blood
395 cell index (β =-0.398; p=0.00056; **Figure 8b**). The presence of prolonged hypoxia
396 around the time of death, as indicated by either low brain pH or high agonal factor
397 score, was associated with a large increase in the endothelial cell index (Agonal Factor:
398 β=0.118 p=2.85e-07; Brain pH: β=-0.210, p= 0.0003; **Figure 8c**) and astrocyte index
399 (Brain pH: β=-0.437, p=2.26e-07; Agonal Factor: β=0.071, p=0.024), matching previous

demonstrations of cerebral angiogenesis, endothelial and astrocyte activation and proliferation in low oxygen environments (41)**.** Small increases were also seen in the mural index in response to low-oxygen (Mural vs. Agonal Factor: β= 0.0493493, p= 0.0286), most likely reflecting angiogenesis. In contrast, prolonged hypoxia was associated with a clear decrease in all of the neuronal indices (Neuron_All vs. Agonal Factor: β=-0.242, p=3.58e-09; Neuron_All vs. Brain pH: β=0.334, p=0.000982; Neuron_Interneuron vs. Agonal Factor: β=-0.078, p=4.13E-05; Neuron_Interneuron vs. Brain pH: β=0.102, p=0.034; Neuron_Projection vs. Agonal Factor: β=-0.096, p= 0.000188), mirroring the notorious vulnerability of neurons to low oxygen (e.g., (42); **Figure 8d**). Finally, we saw a prominent increase in the microglia index in response to low oxygen (Microglia vs. Agonal Factor: β= 0.122096, p= 0.0000181), paralleling known activation of microglia in response to hypoxia (43,44), although we could find little evidence in the literature for actual proliferation under hypoxic events (unlike other injury). This lead us to wonder whether our microglial indices might largely reflect reactive (vs. ramified) microglia since they were typically derived from experiments performed on microglia in dissociated conditions. This possibility was at least partially supported by the presence of many immune-related molecules in the original microglial indices, including many of the interleukins, chemokines, and tumor necrosis factor.

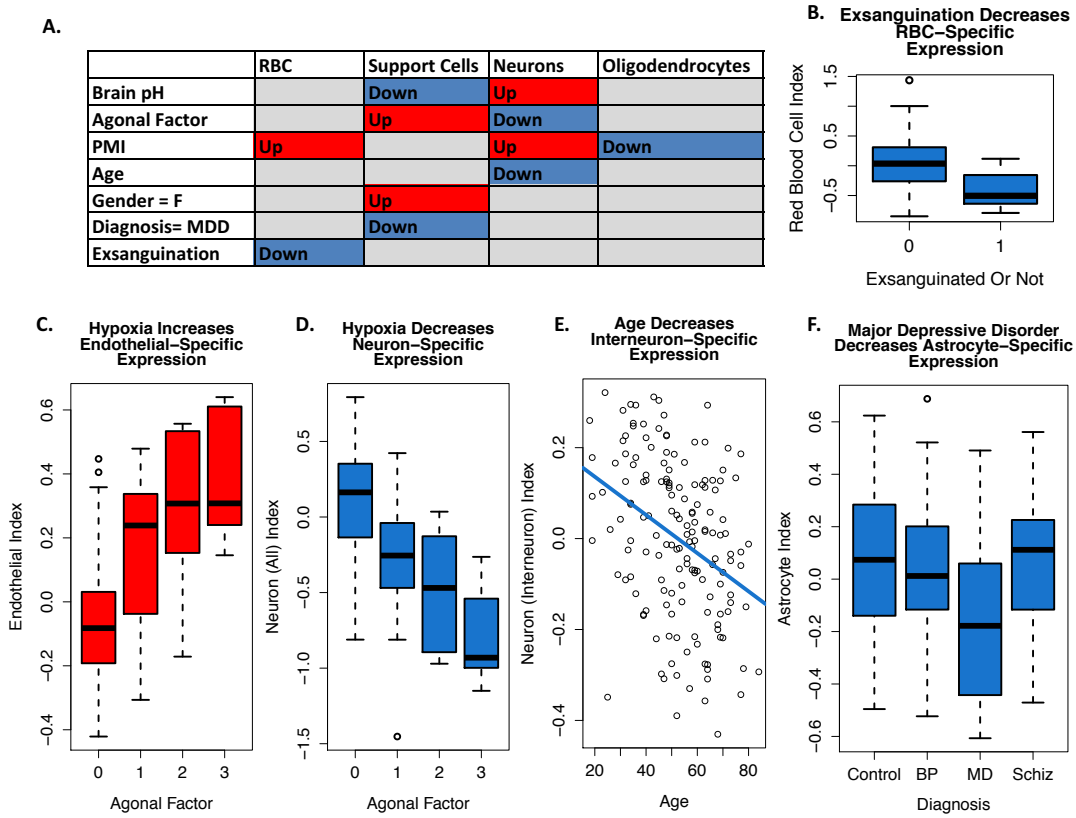

	RBC	Support Cells	Neurons	Oligodendrocytes
Brain pH		Down	Up	
Agonal Factor		Up	Down	
PMI	Up		Up	Down
Age			Down	
Gender = F		Up		
Diagnosis= MDD		Down		
Exsanguination	Down			

Figure 8. Cell content predictions derived from microarray data match known relationships between subject variables and brain tissue cell content. Boxplots represent the median and interquartile range, with whiskers illustrating either the full range of the data or 1.5x the interquartile range. **A.** A table illustrating the relationship between cell types and subject variables ($p<0.05$). General cell type categories showing similar effects have been summarized together ("Support Cells": Astrocytes, Endothelial Cells, Mural Cells, Microglia; "Neurons": Neuron_All, Neuron_Interneuron, Neuron_Projection). Please note that lower pH and higher agonal factor are both indicators of greater hypoxia prior to death, but have an inverted relationship and therefore show opposing relationships with the cell type indices (e.g., when pH is low and agonal factor is high, support cell content is increased). A more detailed table illustrating the relationship between subject variables and each specific cell type can be

found in **Supplementary Figure 14. B.** Subjects that died in a manner that involved exsanguination (n=14) had a notably low red blood cell index (β =-0.398; p=0.00056). **C.** The presence of prolonged hypoxia around the time of death, as indicated by high agonal factor score, was associated with a large increase in the endothelial cell index (Agonal Factor: β=0.118 p=2.85e-07; Brain pH: β=-0.210, p= 0.0003) matching previous demonstrations of cerebral angiogenesis, activation, and proliferation in low oxygen environments (41). **D.** High agonal factor was also associated with a clear decrease in neuronal indices (Neuron_All vs. Agonal Factor: β=-0.242, p=3.58e-09) mirroring the vulnerability of neurons to low oxygen (42). **E.** Age was associated with a moderate decrease in the neuronal indices (Neuron_Interneuron vs. Age: β=- -0.00291, p= 0.000956) which fits known decreases in grey matter density in the frontal cortex in aging humans (45). **F.** Major Depressive Disorder was associated with a moderate decrease in astrocyte index (β = -0.1326572, p= 0.0118), which fits what has been observed morphometrically (46).

Age was associated with a moderate decrease in two of the neuronal indices (Neuron_Interneuron vs. Age: β=- -0.00291, p= 0.000956; Neuron_Projection Neuron vs. Age: β=- 0.00336, p=0.00505; **Figure 8e**), which fits known decreases in gray matter density in the frontal cortex in aging humans (45), as well as age-related sub-region specific decreases in frontal neuron numbers in primates (47) and rats (48). However, in some regions of the prefrontal cortex, age-related decreases in grey matter are primarily driven by synaptic atrophy instead of decreased cell number (49). This

raised the question of whether the decline in our neuronal cell indices with age was being largely driven by the enrichment of genes related to synaptic function in the index.

To explore this possibility, we first evaluated the relationship between age and gene expression while controlling for likely confounds using the signal data for all probesets in the dataset (*Equation 3*, **Figure 5).** We used "DAVID: Functional Annotation Tool" (//david.ncifcrf.gov/summary.jsp, (50,51) to identify the functional clusters that were overrepresented by the genes included in our neuronal cell type indices (using the full HT-U133A chip as background), and then determined the average effect of age (beta) for the genes included in each of the 240 functional clusters (**Suppl. Table 7).** The vast majority of these functional clusters showed a negative relationship with age on average (**Suppl. Figure 13**). However, these functional clusters overrepresented dendritic/axonal related functions, so we blindly chose 29 functional clusters that were clearly related to dendritic/axonal functions and 41 functional clusters that seemed distinctly unrelated to dendritic/axonal functions **(Suppl. Table 7).** Using this approach, we found that transcripts from both classifications of functional clusters showed an average decrease in expression with age (T(28)=-4.5612, *p*= 9.197e-05, T(40)=-2.7566, *p*=0.008756, respectively), but the decrease was larger for transcripts associated with dendritic/axonal-related functions (T(50.082)=2.3385, p= 0.02339, **Suppl. Figure 13**). Based on this analysis, we conclude that synaptic atrophy could be partially driving age-related effects on neuronal cell type indices in the human prefrontal cortex dataset but are unlikely to fully explain the relationship.

Non-canonical relationships between subject variables and predicted cell content can be found in **Figure 8a** and **Suppl. Figure 14.** One of the more prominent

476 unexpected effects was a large decrease in the oligodendrocyte index with longer post-
477 mortem interval (β= - 0.00749, p=0.000474). Upon further investigation, we found a
478 publication documenting a 52% decrease in the fractional anisotropy of white matter
479 with 24 hrs post-mortem interval as detected by neuroimaging (52), but to our
480 knowledge the topic is otherwise not well studied. This effect was accompanied by an
481 increase in two of the neuron indices (Neuron_All vs. PMI: β = 0.006997, p= 0.013509;
482 Neuron_Projection Neuron vs. PMI: β = 0.0070766, p=0.000164), and RBC index (β =
483 0.009612, p= 0.00721), for which we have no good explanation. We also saw an
484 increased mural index (β = 0.0950444, p= 0.00635) and endothelial index (β = 0.06917,
485 p= 0.042738) in females, which, combined with a trend towards increased RBC index
486 (p=0.08) seemed to suggest increased vascularization or meninges, but we could not
487 find any existing support for the hypothesis in the literature.
488 Overall, these results indicate that statistical predictions of the cell content of
489 samples effectively capture known biological changes in cell type balance, and imply
490 that within both chronic (age, sex) and acute conditions (agonal, PMI, pH) there is
491 substantial turbulence in the relative representation of different cell types. Thus, when
492 interpreting microarray data, it is as important to consider demography at the population
493 level as cellular functional regulation.
494

495 ***2.9 Cell Type Balance Changes in Response to Psychiatric Diagnosis***

496 Of most interest to us were potential changes in cell type balance in relation to
497 psychiatric illness. In previous post-mortem morphometric studies, there was evidence
498 of glial loss in the prefrontal cortex of subjects with Major Depressive Disorder, Bipolar

499 Disorder, and Schizophrenia (reviewed in (53)). This decrease in glia, and particularly
500 astrocytes, was replicated experimentally in animals exposed to chronic stress (54), and
501 when induced pharmacologically, was capable of driving animals into a depressive-like
502 condition (54). Replicating the results of (46), we observed a moderate decrease in
503 astrocyte index in the prefrontal cortex of subjects with Major Depressive Disorder (β = -
504 0.1326572, p= 0.0118), but did not see similar changes in the brains of subjects with
505 Bipolar Disorder or Schizophrenia **(Figure 8f).** We did not see significant changes in
506 any of the other cell type indices in relationship to diagnosis.
507

508 ***2.10 Including Cell Content Predictions in the Analysis of Microarray Data***
509 ***Improves the Detection of Diagnosis-Related Genes***

510 Over the years, many researchers have been concerned that transcriptomic and
511 genomic analyses of psychiatric disease often produce non-replicable or contradictory
512 results and, perhaps more disturbingly, are typically unable to replicate well-
513 documented effects detected by other methods. We posited that this lack of sensitivity
514 and replicability might be partially due to cell type variability in the samples, especially
515 since such a large percentage of the principal components of variation in our samples
516 are explained by neuron to glia ratio. Therefore, we compiled a list of genes that had
517 previously documented relationships with psychiatric illness in particular cell types in the
518 human prefrontal cortex, as detected using in situ hybridization, immunocytochemistry,
519 or single-cell laser capture microscopy. These included several genes with a well-
520 documented downregulation in interneurons in relationship to schizophrenia or
521 psychosis (reviewed further in (19); *GAD1*: (55–57); *RELN*:(55); *SST*: (58), *SLC6A1*

522 (*GAT1*): (59), *PVALB*:(56)), and 25 genes recently shown to have highly altered
523 expression in pyramidal neurons in cortical layers 3 and 5 of subjects with
524 schizophrenia using single cell laser capture and microarray (1). We also considered
525 *SYP*, which encodes a protein decreased in projection neurons in subjects with
526 schizophrenia (reviewed further in (19); (60)) and *HTR2A*, which encodes a protein
527 increased in projection neurons in subjects who committed suicide (61). As further
528 validation, it seemed prudent to include genes that were known to have differential
529 expression in relationship with non-psychiatric variables in specific cells within the
530 prefrontal cortex as well. These included *CALB1* and *CALB2,* both of which encode
531 proteins in neurons that decrease with age (62).

532 We then examined our ability to detect these known relationships using models
533 of increasing complexity (**Figure 5**), including a simple base model containing just the
534 variable of interest (*Equation 5,* **Figure 5),** a model controlling for known confounds in
535 the dataset (pH, agonal factor, age, post-mortem interval, and sex, *Equation 3,* **Figure**
536 **5**) and a model controlling for known confounds as well as each of the 10 cell type
537 indices (*Equation 1*, **Figure 5**). Due to the multicollinearity present between the
538 variables included in *Equation 1*, we also used two models that only included the most
539 prevalent cell types (21) and avoided highly correlated categories. The first of these
540 models (*Equation 6,* **Figure 5**) included other major confounds as well, whereas the
541 second model excluded them (*Equation 7,* **Figure 5**).

542 We found that including predictions of cell type balance in our models assessing
543 the effect of diagnosis or age on the expression of our validation genes dramatically
544 improved model fit as assessed by Akaike's Information Criterion (AIC) or Bayesian

545 Information Criterion (BIC), and a 27% reduction in residual standard error (**Figure 9,**
546 **Suppl. Figure 15**). These improvements were largest with the addition of the five most
547 prevalent cell types to the model; the addition of less common cell types produced
548 smaller gains. We also tried replacing the diagnosis term in our models with a more
549 general term representing presence or absence of a psychiatric condition because we
550 had found in the past that many of the genes that were associated with diagnosis in our
551 samples were altered across diagnostic categories. This replacement slightly improved
552 model fit in all versions of the analysis (Eq. 1, 3, 5-7).

553 Overall we found that adding predictions of cell type balance to our models
554 improved our ability to detect previously-documented relationships with diagnosis in the
555 Pritzker dataset (**Figure 9**). Prior to the addition of cell type to the model, we found that
556 only one of 32 genes with a previously documented relationship to diagnosis in
557 individual cells in the prefrontal cortex showed that relationship with a nominal $p<0.05$ in
558 our dataset (*Eq. 5: HTR2A, Eq.1: SLC6A1).* After including cell type balance in the
559 model, the relationship of three genes with diagnosis was now detectable (*SLC6A1,*
560 *SST, COX7B*; **Suppl. Figure 16)**. Overall, the number of validation genes showing the
561 same direction of effect as previously documented increased from 56% (18/32) to 68-
562 72% (23/32). Models that included a more general term for presence or absence of a
563 psychiatric condition performed even better (**Suppl. Figure 17)**. When using a basic
564 model (Eq. 5) or when controlling for known confounds (Eq. 3) only one out of 32
565 validation genes were associated with psychiatric illness (*SLC6A1*). However, once we
566 included predicted cell type balance (Eq. 1) five of the 32 validation genes showed a
567 diagnosis relationship ($p<0.05$, *SST, PVALB, LGALS1, MGST3, ACTR10*), and the

568 percentage of validation genes showing the same direction of effect as previously
569 documented increased from 34% (11/32) to 78% (25/32), a significant improvement as
570 indicated by Fisher's exact test (p=0.036). The use of forward/backward stepwise model
571 selection (using the R function stepwise{Rcmdr}, criterion=BIC) drawing from a pool of
572 variables that included diagnosis, general presence of a psychiatric illness, suicide,
573 known confounds, and all 10 cell types, was also successful at detecting several genes
574 in association with psychiatric illness (*SST, SLC6A1, MGST3, PCSK1*) and suicide
575 (*LGALS1*), but these results should be viewed more cautiously due to the known
576 presence of overfitting in stepwise procedures producing overly optimistic p-values.
577 Backward/forward stepwise selection was noticeably less sensitive and included
578 multiple false positives (incorrect direction of effect with a p<0.05). Both genes with a
579 previously documented relationship to age (*CALB1, CALB2*) had such strong age-
580 related effects in our dataset (*p*=4.84E-23, *p*=8.33E-08, respectively) that model
581 specification had little impact on their results (**Suppl. Figure 18)**.
582

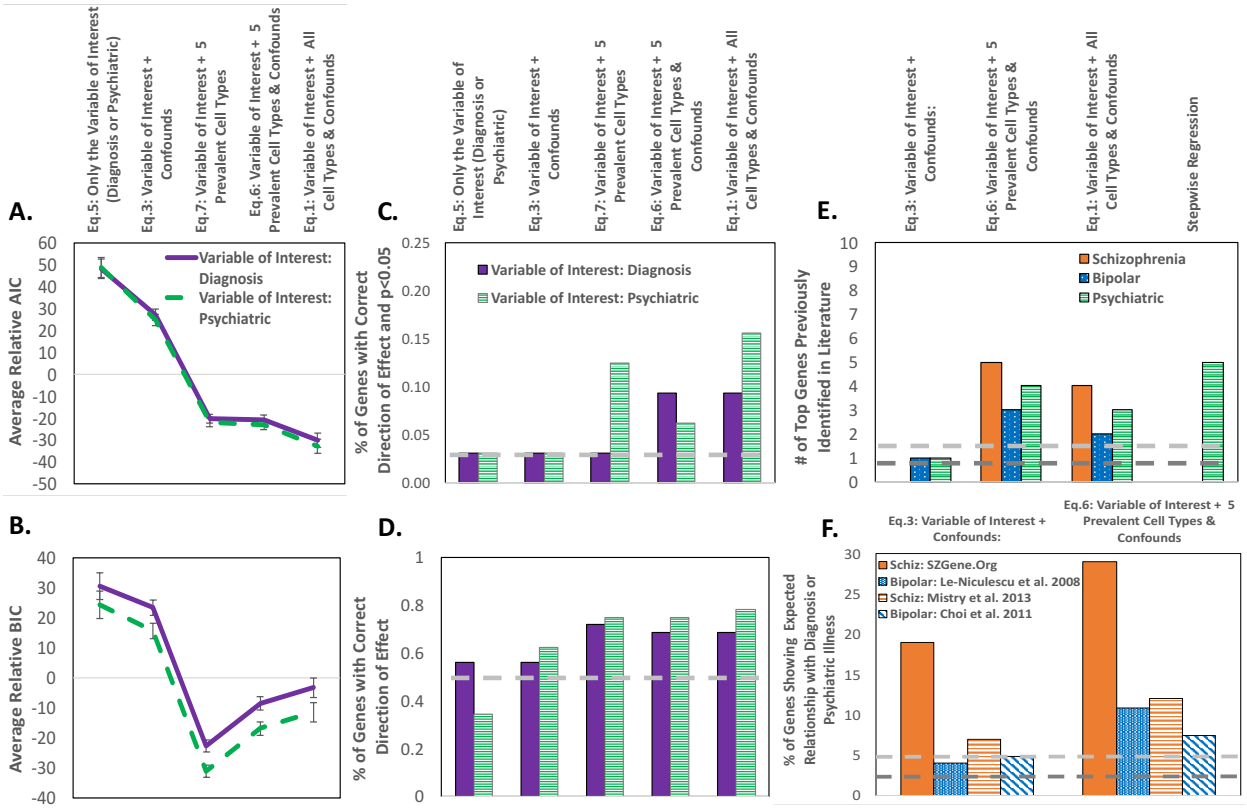

Figure 9. More previously-identified diagnosis-related transcripts are successfully detected by including cell content predictions in the analysis of microarray data. **A-D.** We assessed the fit and sensitivity of five different types of models (arranged in order of complexity) to signal data from 32 genes previously demonstrated to have altered expression or protein content in particular cell types within the dorsolateral prefrontal cortex in relationship to diagnosis (1,19,55–61). Improvements in model fit were largest with the addition of the five most prevalent cell types to the model; the addition of less common cell types produced smaller gains as demonstrated by **A.** Diminishing reductions in AIC with additional model terms (AIC relative to the average for each gene across models, +/-SE), **B.** Lowest BIC for a model that only included psychiatric illness and the five most prevalent cortical cell types (BIC relative to the average for each gene across models, +/-SE). **C.**The addition of cell type to the model

increased the percentage of genes showing the correct relationship with diagnosis or psychiatric illness (with a nominal $p<0.05$) so that it now surpasses what would be expected by random chance (dotted line: 0.05 (nominal p-value)*0.5 (chance of correct direction of effect)). **D.** The addition of cell type to the model increased the percentage of genes showing the correct direction of effect in relationship with diagnosis and psychiatric illness so that it now surpasses what would be expected by random chance (dotted line: 0.5). **E.** When analyzing the full dataset, the top 10 genes associated with diagnosis or psychiatric illness in models that include cell content predictions include genes previously identified in the literature indexed on PubMed. The dotted lines illustrate the rate of overlap with the literature for 100 randomly selected genes from our dataset for Schizophrenia or Bipolar Disorder (grey: 7/100 and 8/100, respectively), or for psychiatric illness in general (dark grey: 15/100, search terms: “Schizophrenia”, “Bipolar”, “Depression”, “Anxiety”, “Suicide”). **F.** The addition of cell type to the model increased the percentage of genes showing the correct relationship with diagnosis or psychiatric illness (with a nominal $p<0.05$) for top genes associated with diagnosis in other types of studies: genome-wide association (63), convergent functional genomics (64), and meta-analyses of macro-dissected microarray (65,66), so that the number of genes showing the expected effects now surpasses what would be expected by random chance (for microarray data: dark grey dotted line: the presence of the relationship and correct direction of effect: 0.05 (nominal p-value)*0.5 (chance of correct direction of effect), for other studies: light grey dotted line: 0.05 for presence of a relationship).

We found that adding predictions of cell type balance to our models also improved our ability to detect altered gene expression associated with known genetic risk loci as well as candidate genes identified by convergent functional genomics, and even enhanced our ability to replicate previous findings from macro-dissected microarray. For example, SZGene.org identified 38 top genes associated with genetic risk loci for Schizophrenia (as reported in (63)), 31 of which were represented in our dataset. Of these, six (19%) were found to have a significant relationship ($p<0.05$) with either Schizophrenia or psychiatric illness in our dataset when controlling for known confounds (Eq.3), whereas nine (29%) were related to either Schizophrenia or psychiatric illness when controlling for known confounds and the most prevalent cell types (*Eq. 6*; Fisher's exact test $p=0.5541$, **Suppl. Fig 19**). Similarly, out of the top 114 genes associated with Bipolar disorder using convergent functional genomics (64), 101 were represented in our dataset. Of these, only four (4%) had a significant relationship ($p<0.05$) with either Bipolar Disorder or psychiatric illness in our dataset when controlling for known confounds, whereas 11 (10.9%) were related to either Bipolar Disorder or psychiatric illness in a model controlling for known confounds and the most prevalent cell types (Fisher's exact test $p=0.1047$, **Suppl. Fig 20**). We had less success identifying altered gene expression in association with the top MDD risk loci identified by (67): out of the 18 genes associated with the 17 SNPs that reached genome-wide significance in their joint analysis of three large sequencing datasets, 12 were represented by probesets in our dataset. Only one of these was found to have a significant relationship with psychiatric illness while accounting for confounds

639 (*SLC6A15*, ß=0.11708, p=0.0302), and no relationships were found when considering
640 confounds and prevalent cell types.

641 We expected that controlling for cell type would weaken our ability to replicate
642 the diagnosis effects observed in other microarray experiments performed on macro-
643 dissected prefrontal tissue, since any changes in cell type balance due to psychiatric
644 illness would be selectively ignored by our analysis. The opposite turned out to be true.
645 For example, (65) found that Bipolar disorder was strongly related to gene expression in
646 the dorsolateral prefrontal cortex data for 400 probes (FDR<0.05), 326 of which
647 represented genes included in our dataset. Of those, only 16 (4.9%) showed the same
648 direction of effect and a p<0.05 in a model including either diagnosis or psychiatric
649 illness and known confounds, whereas 24 (7.4%) showed the same direction of effect
650 and a p<0.05 if the model also included prevalent cell types (Fisher's exact test
651 p=0.2531, **Suppl. Fig 21).** Likewise, (66) found that 125 probes were consistently
652 associated with Schizophrenia in a large meta-analysis of microarray data derived from
653 macro-dissected prefrontal tissue, of which 111 were represented our data set. Of
654 these, eight (7%) showed the same direction of effect and p<0.05 in a model that
655 included either diagnosis or psychiatric illness and known confounds, whereas 13 (12%)
656 showed the same direction of effect and p<0.05 if the model also included the most
657 prevalent cell types (Fisher's exact test= 0.3593, **Suppl. Fig 22**). There was an increase
658 in the number of genes showing the correct direction of effect as well: 50% (psychiatric
659 illness) or 62% (diagnosis) when considering confounds vs. 68% (psychiatric illness) or
660 62% (diagnosis) when considering confounds and prevalent cell types. Altogether,
661 including the most prevalent cell types in our model significantly enhanced our ability to

662 detect relationships between gene expression and diagnosis-related genes identified by
663 a variety of techniques (Fisher's exact test: p=0.0221, **Figure 9F**).
664
665 ***2.11 The Top Diagnosis-Related Genes Identified by Models that Include Cell***
666 ***Content Predictions Pinpoint Known Risk Candidates***
667 Although the inclusion of predicted cell type balance in our model improved our
668 ability to detect previously-identified relationships with diagnosis, most relationships still
669 went undetected and none of the diagnosis relationships survived standard p-value
670 corrections for multiple comparisons when included in a full microarray analysis. This
671 could be due to a variety of factors, including microarray platform and probe sensitivity
672 as well as the possibility that other cell types in the dataset are showing effects in a
673 competing direction. Therefore, we decided to ask a complementary question: Of the
674 top diagnosis relationships that we see in our dataset, how many have been previously
675 observed in the literature? If including predicted cell type balance in our models
676 improves the signal to noise ratio of our analyses, then we would expect that the top
677 diagnosis-related genes in our dataset would be more likely to overlap with previous
678 findings. In an attempt to perform this comparison in an unbiased and efficient manner,
679 we limited our search to PubMed, using as search terms only the respective human
680 gene symbol and diagnosis ("Schizophrenia", "Bipolar", or "Depression"). For the genes
681 related to MDD in our dataset, we also expanded the search to include two highly-
682 correlated traits that are more quantifiable and likely to have a genetic basis: "Anxiety"
683 and "Suicide". Then we narrowed our results only to studies using human subjects.

We found that only one of the top 10 diagnosis-related genes detected using a model that included diagnosis and known confounds (*Equation 3)* was previously noted in the human literature *(FOS:* (68,69)). The same was true if we replaced diagnosis with a term representing the general presence or absence of a psychiatric illness (*ALDH1A1:* (64)). In contrast, when we used a model that included diagnosis, known confounds, and predictions for the balance of the five most prevalent cortical cell types (*Equation 6*), we found that five of the top 10 genes associated with Schizophrenia had been previously identified in the literature (*ARHGEF2:* (70)**,** *DOC2A:* (71), *FBX09:* (66), *GRM1:* (72,73); *CEBPA:* (74)), and three of the top 10 genes associated with Bipolar Disorder (*ALDH1A1:* (64)**,** *SNAP25:* (75), *NRN1:*(76)**; Suppl. Figure 23, Suppl. Table 8, Suppl. Table 10**). This was a significant enrichment in overlap with the literature as indicated by a Fisher's exact test across all three diagnosis groups (1/30 vs. 8/30 overlap with the literature, p=0.0257, **Figure 9E**) or when comparing the results for the schizophrenia group to the rate of overlap with the literature for 100 randomly-selected genes in the dataset subjected to the same protocol (Schizophrenia: 5/10 vs. 7/100, p=0.0012; Bipolar: 3/10 vs. 8/100, p=0.0610). Likewise, if we replaced diagnosis with a term representing the general presence or absence of a psychiatric illness, we found that four of the top 10 genes had been previously identified in the literature (*ALDH1A1*: (64); *HBS1L:* (4); *HIVEP2:* (77), *FBX09*: (66), **Suppl. Figure 24, Suppl. Table 9, Suppl. Table 11**), and 9/10 of the top genes were actually significant with an FDR<0.05 when using permutation based methods (using the R function lmp{lmPerm}, iterations=9999). The top 10 genes associated with psychiatric illness in models selected using forward/backward stepwise model selection (criterion=BIC) similarly included five that

707 had been previously identified in the literature (*PRSS16:* (63), *GRM1:* (72,73);
708 *ALDH1A1:* (64); *SNAP25:* (75); *HIVEP2:* (77), a significant improvement in overlap with
709 the literature than what can be seen in 100 randomly-selected genes in the dataset
710 subjected to the same protocol (Fisher's exact test: 5/10 vs.15/100, p=0.0168).
711 Together, we conclude that including cell content predictions in the analysis of
712 macro-dissected microarray data improves the sensitivity of the assay for detecting
713 altered gene expression in relationship to psychiatric disease.
714
715 **3. Discussion**
716
717 In this manuscript, we have demonstrated that the statistical cell type index is a
718 relatively simple manner of interrogating cell-type specific expression in transcriptomic
719 datasets from macro-dissected human brain tissue. We find that statistical estimations
720 of cell type balance almost fully account for the principal components of variation in
721 microarray data derived from macrodissected brain tissue samples, far surpassing the
722 importance of other subject variables (post-mortem interval, hypoxia, age, gender).
723 Indeed, our results suggest that many variables of medical interest are themselves
724 accompanied by strong changes in cell type composition in naturally-observed human
725 brains. We find that within both chronic (age, sex, diagnosis) and acute conditions
726 (agonal, PMI, pH) there is substantial turbulence in the relative representation of
727 different cell types. Thus, accounting for demography at the cellular population level is
728 as important for the interpretation of microarray data as cell-level functional regulation.
729 This form of data deconvolution was particularly useful for identifying the subtler effects

730 of psychiatric illness within our samples, divulging the decrease in astrocytes that is
731 known to occur in Major Depressive Disorder, and doubling the sensitivity of our assay
732 to detect previously-identified diagnosis-related genes.

733 These results touch upon the fundamental question as to whether organ-level
734 function responds to challenge by changing the biological states of individual cells
735 (Lamarckian) or the life and death of different cell populations (Darwinian). To reach
736 such a sweeping perspective in human brain tissue using classic cell biology methods
737 would require epic efforts in labeling, cell sorting, and counting. We have demonstrated
738 that you can approximate this vantage point using an elegant, supervised signal
739 decomposition exploiting increasingly available genomic data. However, it should be
740 noted that, similar to other forms of functional annotation, cell type indices are best
741 treated as a *hypothesis-generation tool* instead of a final conclusion regarding tissue
742 cell content. We have demonstrated the utility of cell type indices for detecting strong
743 effects in a microarray dataset, including other genes with highly cell-type specific
744 expression and large-scale alterations in cell content in relationship with known subject
745 variables. We have not tested the sensitivity of the technique for detecting smaller
746 effects or parsing effects for genes related to multiple cell types, or the validity under all
747 circumstances or non-cortical tissue types. Likewise, while using this technique it is
748 impossible to distinguish between alterations in cell type balance and cell-type specific
749 transcriptional activity: when a sample shows a higher value of a particular cell type
750 index, it could have a larger number of such cells, or each cell could have produced
751 more of its unique group of transcripts, via a larger cell body, slower mRNA
752 degradation, or an overall change in transcription rate. In this regard the index that we

753 calculate does not have a specific interpretation; rather it is a holistic property of the cell
754 populations, the “neuron-ness” or “microglia-ness” of the sample. Such an abstract
755 index represents the ecological shifts inferred from the pooled transcriptome. That said,
756 unlike principal component scores or other associated techniques of removing
757 unwanted variation from genomic data, our cell type indices do have real biological
758 meaning - they can be interpreted in a known system of cell type taxonomy. When
759 single-cell genomic data uncovers new cell types (e.g., the Allen Brain Atlas cellular
760 taxonomy initiative (78)) or meta-analyses refine the list of genes defined as having cell-
761 type specific expression (e.g., (79)), our indices will surely evolve with these new
762 classification frameworks, but the power of our approach will remain, in that we can
763 disentangle the intrinsic changes of individual genes from the population-level shifts of
764 major cell types. The same approach can be extended to studying other structurally
765 complex organs that involve the concerted function of many cell types.

766 Although we generated our method independently to address microarray analysis
767 questions that arose within the Pritzker Neuropsychiatric Consortium, we later
768 discovered that it was quite similar to the technique of population-specific expression
769 analysis (PSEA) introduced by (12) with several notable differences. Similar to our
770 method, PSEA aims to estimate cell type-differentiated disease effects from microarray
771 data derived from brain tissue of heterogeneous composition and approaches this
772 problem by including the averaged, normalized expression of cell type specific markers
773 within a larger linear model that is used to estimate differential expression in microarray
774 data. Likewise, using PSEA, (12) also found that individual variability in neuronal,
775 astrocytic, oligodendrocytic, and microglial cell content was sufficient to account for

substantial variability in the vast majority of probe sets, even within non-diseased samples. Most importantly, the PSEA technique has been carefully validated: PSEA was found to successfully predict the content of RNA-mixing experiments (12), cellular expression data from *in situ* hybridization or laser-capture microdissection experiments (11), and neuron-specific neurodegenerative effects found with laser-capture microdissection (10).The differences between our techniques are mostly due to our access to a large sample size and the recent growth of the literature documenting cell type specific expression in brain cell types. PSEA uses a very small set of markers (4-7) to represent each cell type, and screens these markers for tight co-expression within the dataset of interest, since co-expression networks have been previously demonstrated to often represent cell type signatures in the data (80). This is essential for the analysis of microarray data for brain regions that have not been well characterized for cell type specific expression (*e.g.,* the substantia nigra), but risks the possibility of closely tracking variability in a particular cell function instead of cell content (as described in our results related to aging). Our analysis predominantly focused on the well-studied cortex, thus enabling us to expand our analysis to include hundreds of cell type specific markers derived from a variety of experimental techniques. Likewise, PSEA was designed for use with small microarray datasets, and thus depends on a variety of model selection techniques to minimize the number of terms included in the linear model. Although necessary, this step introduces the risk of mis-assigning effects associated with correlated cell types. Using a large dataset gave us the opportunity to include terms for all major cell types in the analysis, as well as terms representing a number of important identified confounds (age, pH, PMI, gender). Due to these

799 analytical differences, we are able to effectively characterize gene expression
800 associated with less prevalent cell types (*e.g.,* endothelial cells) and compare the utility
801 of cell type specific markers derived from a variety of species and experimental
802 techniques.

803 There was one seemingly-small difference between our method and PSEA that
804 actually turned out to produce a large difference in efficacy: normalization of the original
805 gene expression data using a z-score instead of a ratio of the mean (81). As part of a
806 set of later validation analyses (**Suppl. Methods and Results, Suppl. Figures 25-26**),
807 we performed a head-to-head comparison of our method and PSEA using a single-cell
808 RNA-Seq dataset and the same database of cell type specific genes. Both methods
809 strongly predicted cell identity, but on average we found that one third of the variation in
810 the predictions of relative cell content derived from PSEA ("population reference signal")
811 were related to the cell identity of the samples versus almost half of the variation in our
812 consolidated cell type indices. We conclude that our method may be a more effective
813 manner of predicting cell type balance in some datasets.

814 Another notable difference between our final analysis methods and those used
815 by PSEA (10–12) was the lack of cell type interaction terms included in our models
816 (*e.g., Diagnosis*Astrocyte Index*). Theoretically, the addition of cell type interaction
817 terms should allow the researcher to statistically interrogate cell-type differentiated
818 diagnosis effects because samples that contain more of a particular cell type should
819 exhibit more of that cell type's respective diagnosis effect. Versions of this form of
820 analysis have been successful in other investigations (e.g., (11,12,82)) but we were not
821 able to validate the method using our database of previously-documented relationships

822 with diagnosis in prefrontal cell types and a variety of model specifications (e.g., **Suppl.**
823 **Figure 27)**. Upon consideration, we realized that these negative results were difficult to
824 interpret because significant diagnosis*cell type interactions should only become
825 evident if the effect of diagnosis in a particular cell type is different from what is
826 occurring in all cell types on average. For genes with expression that is reasonably
827 specific to a particular cell type (*e.g.,* GAD1), the overall average diagnosis effect may
828 already largely reflect the effect within that cell type and the respective interaction term
829 will not be significantly different, even though the disease effect is clearly tracking the
830 balance of that cell population. In the end, we decided that the addition of interaction
831 terms to our models was not demonstrably worth the associated decrease in overall
832 model fit and statistical power.

833 One result from our analysis seems particularly worth discussing in greater
834 depth. It has been acknowledged for a long time that exposure to a hypoxic
835 environment prior to death has a huge impact on gene expression in human post-
836 mortem brains (e.g., (25,26,83,84)). This impact on gene expression is so large that up
837 until recently the primary principal component of variation (PC1) in our Pritzker data was
838 assumed to represent the degree of hypoxia, and was sometimes even systematically
839 removed before performing diagnosis-related analyses (e.g., (85)). However, the
840 magnitude of the effect of hypoxia was puzzling, especially when compared to the much
841 more moderate effects of post-mortem interval, even when the intervals ranged from 8-
842 40+ hrs. Our current analysis provides an explanation for this discrepancy, since it is
843 clear from our results that the brains of our subjects are actively compensating for a
844 hypoxic environment prior to death by altering the balance or overall transcriptional

activity of support cells and neurons. Although the differential effects of hypoxia on neurons and glial cells have been studied since the 1960's (86), to our knowledge this is the first time that anyone has related the large effects of hypoxia in post-mortem transcriptomic data to alterations in cell type balance in the samples. This connection is important for understanding why results associating gene expression and psychiatric illness in human post-mortem tissue sometimes do not replicate. If a study contains mostly tissue from individuals who experienced greater hypoxia before death (*e.g.,* hospital care with artificial respiration or drug overdose followed by coma), then the evaluation of the effect of neuropsychiatric illness is likely to inadvertently focus on differential expression in support cell types (astrocytes, endothelial cells), whereas a study that mostly contains tissue from individuals who died a fast death (*e.g.,* car accident or myocardial infarction) will emphasize the effects of neuropsychiatric illness in neurons.

Finally, our work drives home the fact that any comprehensive theory of psychiatric illness needs to account for the dichotomy between the health of individual cells and that of their ecosystem. We found that the functional changes accompanying psychiatric illness in the dorsolateral prefrontal cortex occurred both at the level of cell population shifts (decreased astrocytic presence) and at the level of intrinsic gene regulation not explained by population shifts. A similar conclusion regarding the importance of cell type balance in association with psychiatric illness was recently drawn by our collaborators (*e.g.,*(87)) using a similar technique to analyze RNA-Seq data from the anterior cingulate cortex. In the future, we plan to use our technique to re-analyze many of the other large microarray datasets existing within the Pritzker

868 Neuropsychiatric Consortium with the hope of gaining better insight into psychiatric
869 disease effects. This application of our technique seems particularly important in light of
870 recent evidence linking disrupted neuroimmunity (74) and neuroglia (*e.g.,* (46,54,88)) to
871 psychiatric illness, as well as growing evidence that growth factors with cell type specific
872 effects play an important role in depressive illness and emotional regulation (*e.g.,* Brain-
873 Derived Neurotrophic Factor (*BDNF*), the Fibroblast Growth Factor (*FGF*) family, Glial-
874 cell derived neurotrophic factor (*GDNF*), Vascular Endothelial Growth Factor (*VEGF*);
875 for a review, see (23,89)).

876 In conclusion, we have found this method to be a valuable addition to traditional
877 functional ontology tools as a manner of improving the interpretation of transcriptomic
878 results as well as removing unwanted noise due to variations in cell content caused by
879 dissection variability. The capability to unravel alterations of cell type composition from
880 modulation of cell state, even just probabilistically, is inherently useful for understanding
881 the higher-level function of the brain as emergent properties of brain activity, such as
882 emotion, cognition, memory, and addiction, usually involve ensembles of many cells.
883 Facilitating the interpretation of gene activity data in macro-dissected tissue in light of
884 both processes provides new opportunities to integrate results with findings from other
885 approaches, such as electrophysiology analysis of brain circuits, brain imaging,
886 optogenetic manipulations, and naturally occurring variation in response to injury and
887 brain diseases.

888 For the benefit of other researchers, we have made our database of brain cell
889 type specific genes (https://sites.google.com/a/umich.edu/megan-hastings-
890 hagenauer/home/cell-type-analysis) and R code for conducting cell type analyses

891 publically available in the form of a downloadable R package
892 (https://github.com/hagenaue/BrainInABlender) and we are happy to assist researchers
893 in their usage for pursuing better insight into psychiatric illness and neurological
894 disease.
895
896 **4. Materials and Methods**
897
898 ***4.1 Ortholog Prediction:*** The gene symbols for the cell type specific transcripts derived
899 from mouse datasets were fed into HCOP: Orthology Prediction Search
900 (http://www.genenames.org/cgi-bin/hcop). We selected the ortholog for each transcript
901 that was most commonly identified amongst the 11 available databases: EggNOG,
902 Ensembl, HGNC, HomoloGene, Inparanoid, OMA, OrthoDB, OrthoMCL, Panther,
903 PhylomeDB, and TreeFam.
904
905 ***4.2 Pritzker Dorsolateral Prefrontal Cortex Microarray Dataset:***
906 The original dataset included tissue from 172 high-quality human post-mortem
907 brains donated to the Brain Donor Program at the University of California, Irvine with the
908 consent of the next of kin. Frozen coronal slabs were macro-dissected to obtain
909 dorsolateral prefrontal cortex samples and total RNA was extracted and hybridized to
910 Affymetrix HT-U133A or HT-U133Plus-v2 chips in duplicate or triplicate at different
911 laboratories using procedures described previously (25,85). Clinical information was
912 obtained from medical examiners, coroners' medical records, and a family member.
913 Patients were diagnosed with either Major Depressive Disorder, Bipolar Disorder, or

Schizophrenia by consensus based on criteria from the Diagnostic and Statistical Manual of Mental Disorders (90). Data from any subjects lacking information regarding critical pre- or post-mortem variables were removed from the analysis, leaving a final sample size of *n=157.* For detailed data collection methodology, see (85). This research was overseen and approved by the University of Michigan Institutional Review Board (IRB # HUM00043530, Pritzker Neuropsychiatric Disorders Research Consortium (2001-0826)) and the University of California Irvine (UCI) Institutional Review Board (IRB# 1997-74).

Before conducting the current analysis, the microarray dataset was reannotated for probe-to-transcript correspondance (91), summarized using robust multi-array analysis (RMA) (92), log (base 2)-transformed, quantile normalized, gender-checked, median centered to remove batch effects, and the replicate microarrays for each subject were averaged (for a more detailed description of data preprocessing see (85)). Samples that exhibited markedly low average sample-sample correlation coefficients prior to median centering (<0.85: outliers) were removed from the dataset, including data from one batch that exhibited overall low sample-sample correlation coefficients with other batches and poor match with their duplicate microarrays run in a separate laboratory.

The data from control subjects is publically available in the Gene Expression Omnibus (GEO: Accession Number GSE6306) and the data for all subjects has been submitted and should be available shortly (GEO: *curation pending*) . All of the R script documenting these analyses can be found at https://github.com/hagenaue/CellTypeAnalyses_PritzkerAffyDLPFC.

937

938 ***4.3 Allen Brain Atlas Cross-Regional Microarray Dataset:***

939 The Allen Brain Atlas microarray data was downloaded from http://human.brain-
940 map.org/microarray/search on December 2015. This microarray survey was performed
941 in brain-specific batches, with multiple batches per subject. To remove technical
942 variation across batches, a variety of normalization procedures had been performed by
943 the original authors both within and across batches using internal controls, as well as
944 across subjects (93). The dataset available for download had already been log-
945 transformed (base 2) and converted to z-scores using the average and standard
946 deviation for each probe. These normalization procedures were designed to remove
947 technical artifacts while best preserving cross-regional effects in the data, but the full
948 information about relative levels of expression within an individual sample were
949 unavailable and the effects of subject-level variables (such as age and pH) were likely
950 to be de-emphasized due to the inability to fully separate out subject and batch during
951 the normalization process.

952 Prior to conducting other analyses, we averaged the expression level of the
953 multiple probes that corresponded to the same gene, and re-scaled, so that the data
954 associated with each gene symbol continued to be a z-score (mean=0, sd=1). We then
955 extracted the z-score data for the list of cell type specific genes derived from each
956 publication. Based on our results from analyzing the Pritzker dataset, we excluded the
957 data for genes that were non-specific (i.e., included in a list of cell type specific genes
958 from a different category of cells within any of the publications), and then averaged the
959 data from the cell-type specific genes derived from each publication to predict the

relative content of each of the 10 primary cell types in each sample. All of the R script documenting these analyses can be found at https://github.com/hagenaue/CellTypeAnalyses_AllenBrainAtlas.

5. Acknowledgements

We thank all the members of the Pritzker Consortium (especially the University of California, Irvine Brain Bank staff), Drs. Adriana Medina and David Krolewski for brain dissections and methodological input, and Dr. Simon Evans, Sharon Burke and Mary Hoverstein for their involvement in the initial mRNA extraction and microarrays. Grace Hsienyuan Chang, Jennifer Fitzpatrick, LeAnn Fitzpatrick, Jim Stewart, Tom Dixon, Doug Smith, Andy Lin, and Manhong Dai were invaluable for maintaining our databases of clinical information and biological specimens. We would also like to thank Drs. Elyse Aurbach, Katherine Prater, Kathryn Hilde, Fan Meng, and Mark Reimers for advice and feedback regarding the methodology or manuscript. Finally, we would also like to thank our undergraduate research assistants Isabelle Birt, Alek Pankonin, and Daniela Romero Vargas for their help compiling the Allen Brain Atlas data, annotating and uploading code, creating the BrainInABlender R package, and editorial assistance.

6. References

1. Arion D, Corradi JP, Tang S, Datta D, Boothe F, He A, et al. Distinctive transcriptome alterations of prefrontal pyramidal neurons in schizophrenia and schizoaffective disorder. Mol Psychiatry. 2015 Nov;20(11):1397–405.

2. Darmanis S, Sloan SA, Zhang Y, Enge M, Caneda C, Shuer LM, et al. A survey of human brain transcriptome diversity at the single cell level. Proc Natl Acad Sci U S A. 2015 Jun 9;112(23):7285–90.

3. Lake BB, Ai R, Kaeser GE, Salathia NS, Yung YC, Liu R, et al. Neuronal subtypes and diversity revealed by single-nucleus RNA sequencing of the human brain. Science. 2016 Jun 24;352(6293):1586–90.

989 4. Choi KH, Elashoff M, Higgs BW, Song J, Kim S, Sabunciyan S, et al. Putative psychosis
990 genes in the prefrontal cortex: combined analysis of gene expression microarrays.
991 BMC Psychiatry. 2008;8:87.

992 5. Evans SJ, Choudary PV, Neal CR, Li JZ, Vawter MP, Tomita H, et al. Dysregulation of the
993 fibroblast growth factor system in major depression. Proc Natl Acad Sci U S A. 2004
994 Oct 26;101(43):15506–11.

995 6. Abbas AR, Wolslegel K, Seshasayee D, Modrusan Z, Clark HF. Deconvolution of blood
996 microarray data identifies cellular activation patterns in systemic lupus
997 erythematosus. PloS One. 2009;4(7):e6098.

998 7. Chikina M, Zaslavsky E, Sealfon SC. CellCODE: a robust latent variable approach to
999 differential expression analysis for heterogeneous cell populations. Bioinforma Oxf
1000 Engl. 2015 May 15;31(10):1584–91.

1001 8. Gaujoux R, Seoighe C. CellMix: a comprehensive toolbox for gene expression
1002 deconvolution. Bioinforma Oxf Engl. 2013 Sep 1;29(17):2211–2.

1003 9. Shen-Orr SS, Gaujoux R. Computational deconvolution: extracting cell type-specific
1004 information from heterogeneous samples. Curr Opin Immunol. 2013 Oct;25(5):571–8.

1005 10. Capurro A, Bodea L-G, Schaefer P, Luthi-Carter R, Perreau VM. Computational
1006 deconvolution of genome wide expression data from Parkinson's and Huntington's
1007 disease brain tissues using population-specific expression analysis. Front Neurosci.
1008 2014;8:441.

1009 11. Kuhn A, Kumar A, Beilina A, Dillman A, Cookson MR, Singleton AB. Cell population-
1010 specific expression analysis of human cerebellum. BMC Genomics. 2012;13:610.

1011 12. Kuhn A, Thu D, Waldvogel HJ, Faull RLM, Luthi-Carter R. Population-specific
1012 expression analysis (PSEA) reveals molecular changes in diseased brain. Nat Methods.
1013 2011 Nov;8(11):945–7.

1014 13. Cahoy JD, Emery B, Kaushal A, Foo LC, Zamanian JL, Christopherson KS, et al. A
1015 transcriptome database for astrocytes, neurons, and oligodendrocytes: a new resource
1016 for understanding brain development and function. J Neurosci Off J Soc Neurosci. 2008
1017 Jan 2;28(1):264–78.

1018 14. Daneman R, Zhou L, Agalliu D, Cahoy JD, Kaushal A, Barres BA. The mouse blood-brain
1019 barrier transcriptome: a new resource for understanding the development and
1020 function of brain endothelial cells. PloS One. 2010;5(10):e13741.

1021 15. Doyle JP, Dougherty JD, Heiman M, Schmidt EF, Stevens TR, Ma G, et al. Application of a
1022 translational profiling approach for the comparative analysis of CNS cell types. Cell.
1023 2008 Nov 14;135(4):749–62.

1024 16. Sugino K, Hempel CM, Miller MN, Hattox AM, Shapiro P, Wu C, et al. Molecular
1025 taxonomy of major neuronal classes in the adult mouse forebrain. Nat Neurosci. 2006
1026 Jan;9(1):99–107.

1027 17. Zeisel A, Muñoz-Manchado AB, Codeluppi S, Lönnerberg P, La Manno G, Juréus A, et al.
1028 Brain structure. Cell types in the mouse cortex and hippocampus revealed by single-
1029 cell RNA-seq. Science. 2015 Mar 6;347(6226):1138–42.

1030 18. Zhang Y, Chen K, Sloan SA, Bennett ML, Scholze AR, O'Keeffe S, et al. An RNA-
1031 sequencing transcriptome and splicing database of glia, neurons, and vascular cells of
1032 the cerebral cortex. J Neurosci Off J Soc Neurosci. 2014 Sep 3;34(36):11929–47.

1033 19. Lewis DA, Sweet RA. Schizophrenia from a neural circuitry perspective: advancing
1034 toward rational pharmacological therapies. J Clin Invest. 2009 Apr;119(4):706–16.

1035 20. Lynch JC. The Cerebral Cortex. In: Fundamental Neuroscience. 2nd ed. Philadelphia:
1036 Churchill Livingstone; 2002. p. 505–20.

1037 21. Hutchins DE, Naftel JP, Ard MD. The cell biology of neurons and glia. In: Fundamental
1038 Neuroscience. 2nd ed. Philadelphia: Churchill Livingstone; 2002. p. 15–36.

1039 22. Bergers G, Song S. The role of pericytes in blood-vessel formation and maintenance.
1040 Neuro-Oncol. 2005 Oct;7(4):452–64.

1041 23. Duman RS, Monteggia LM. A neurotrophic model for stress-related mood disorders.
1042 Biol Psychiatry. 2006 Jun 15;59(12):1116–27.

1043 24. Doss JF, Corcoran DL, Jima DD, Telen MJ, Dave SS, Chi J-T. A comprehensive joint
1044 analysis of the long and short RNA transcriptomes of human erythrocytes. BMC
1045 Genomics. 2015;16(1):952.

1046 25. Li JZ, Vawter MP, Walsh DM, Tomita H, Evans SJ, Choudary PV, et al. Systematic
1047 changes in gene expression in postmortem human brains associated with tissue pH
1048 and terminal medical conditions. Hum Mol Genet. 2004 Mar 15;13(6):609–16.

1049 26. Tomita H, Vawter MP, Walsh DM, Evans SJ, Choudary PV, Li J, et al. Effect of agonal and
1050 postmortem factors on gene expression profile: quality control in microarray analyses
1051 of postmortem human brain. Biol Psychiatry. 2004 Feb 15;55(4):346–52.

1052 27. Wilkerson MD, Hayes DN. ConsensusClusterPlus: a class discovery tool with
1053 confidence assessments and item tracking. Bioinforma Oxf Engl. 2010 Jun
1054 15;26(12):1572–3.

1055 28. Coupel S, Moreau A, Hamidou M, Horejsi V, Soulillou J-P, Charreau B. Expression and
1056 release of soluble HLA-E is an immunoregulatory feature of endothelial cell activation.
1057 Blood. 2007 Apr 1;109(7):2806–14.

1058 29. Tian H, McKnight SL, Russell DW. Endothelial PAS domain protein 1 (EPAS1), a
1059 transcription factor selectively expressed in endothelial cells. Genes Dev. 1997 Jan
1060 1;11(1):72–82.

1061 30. Tchorz JS, Tome M, Cloëtta D, Sivasankaran B, Grzmil M, Huber RM, et al. Constitutive
1062 Notch2 signaling in neural stem cells promotes tumorigenic features and astroglial
1063 lineage entry. Cell Death Dis. 2012;3:e325.

1064 31. Boyles JK, Pitas RE, Wilson E, Mahley RW, Taylor JM. Apolipoprotein E associated with
1065 astrocytic glia of the central nervous system and with nonmyelinating glia of the
1066 peripheral nervous system. J Clin Invest. 1985 Oct;76(4):1501–13.

1067 32. Fazzari P, Paternain AV, Valiente M, Pla R, Luján R, Lloyd K, et al. Control of cortical
1068 GABA circuitry development by Nrg1 and ErbB4 signalling. Nature. 2010 Apr
1069 29;464(7293):1376–80.

1070 33. Stephenson DT, Coskran TM, Kelly MP, Kleiman RJ, Morton D, O'Neill SM, et al. The
1071 distribution of phosphodiesterase 2A in the rat brain. Neuroscience. 2012 Dec
1072 13;226:145–55.

1073 34. Marszalek JR, Weiner JA, Farlow SJ, Chun J, Goldstein LS. Novel dendritic kinesin
1074 sorting identified by different process targeting of two related kinesins: KIF21A and
1075 KIF21B. J Cell Biol. 1999 May 3;145(3):469–79.

1076 35. Hawrylycz MJ, Lein ES, Guillozet-Bongaarts AL, Shen EH, Ng L, Miller JA, et al. An
1077 anatomically comprehensive atlas of the adult human brain transcriptome. Nature.
1078 2012 Sep 20;489(7416):391–9.

1079 36. Allen Brain Atlas. Technical White Paper: Case qualification and donor profiles, v.7
1080 [Internet]. 2013. Available from: help.brain-map.org

1081 37. Allen Brain Atlas. Technical White Paper: Microarray Survey, v.7 [Internet]. 2013.
1082 Available from: help.brain-map.org

1083 38. Carpenter MB. Core Text of Neuroanatomy. 4th ed. Baltimore, MD: Williams & Wilkins;
1084 1991.

1085 39. Altman J, Das GD. Autoradiographic and histological evidence of postnatal
1086 hippocampal neurogenesis in rats. J Comp Neurol. 1965 Jun;124(3):319–35.

1087 40. Amaral DG, Scharfman HE, Lavenex P. The dentate gyrus: fundamental
1088 neuroanatomical organization (dentate gyrus for dummies). Prog Brain Res.
1089 2007;163:3–22.

1090 41. Li L, Welser JV, Dore-Duffy P, del Zoppo GJ, Lamanna JC, Milner R. In the hypoxic
1091 central nervous system, endothelial cell proliferation is followed by astrocyte

1092 activation, proliferation, and increased expression of the alpha 6 beta 4 integrin and
1093 dystroglycan. Glia. 2010 Aug;58(10):1157–67.

1094 42. Banasiak KJ, Haddad GG. Hypoxia-induced apoptosis: effect of hypoxic severity and
1095 role of p53 in neuronal cell death. Brain Res. 1998 Jun 29;797(2):295–304.

1096 43. Lu D-Y, Liou H-C, Tang C-H, Fu W-M. Hypoxia-induced iNOS expression in microglia is
1097 regulated by the PI3-kinase/Akt/mTOR signaling pathway and activation of hypoxia
1098 inducible factor-1alpha. Biochem Pharmacol. 2006 Oct 16;72(8):992–1000.

1099 44. Tadmouri A, Champagnat J, Morin-Surun MP. Activation of microglia and astrocytes in
1100 the nucleus tractus solitarius during ventilatory acclimatization to 10% hypoxia in
1101 unanesthetized mice. J Neurosci Res. 2014 May;92(5):627–33.

1102 45. Sowell ER, Peterson BS, Thompson PM, Welcome SE, Henkenius AL, Toga AW.
1103 Mapping cortical change across the human life span. Nat Neurosci. 2003
1104 Mar;6(3):309–15.

1105 46. Rajkowska G, Miguel-Hidalgo JJ, Wei J, Dilley G, Pittman SD, Meltzer HY, et al.
1106 Morphometric evidence for neuronal and glial prefrontal cell pathology in major
1107 depression. Biol Psychiatry. 1999 May 1;45(9):1085–98.

1108 47. Smith DE, Rapp PR, McKay HM, Roberts JA, Tuszynski MH. Memory impairment in
1109 aged primates is associated with focal death of cortical neurons and atrophy of
1110 subcortical neurons. J Neurosci Off J Soc Neurosci. 2004 May 5;24(18):4373–81.

1111 48. Stranahan AM, Jiam NT, Spiegel AM, Gallagher M. Aging reduces total neuron number
1112 in the dorsal component of the rodent prefrontal cortex. J Comp Neurol. 2012 Apr
1113 15;520(6):1318–26.

1114 49. Peters A, Sethares C, Luebke JI. Synapses are lost during aging in the primate
1115 prefrontal cortex. Neuroscience. 2008 Apr 9;152(4):970–81.

1116 50. Huang DW, Sherman BT, Zheng X, Yang J, Imamichi T, Stephens R, et al. Extracting
1117 biological meaning from large gene lists with DAVID. Curr Protoc Bioinforma Ed Board
1118 Andreas Baxevanis Al. 2009 Sep;Chapter 13:Unit 13.11.

1119 51. Huang DW, Sherman BT, Lempicki RA. Systematic and integrative analysis of large
1120 gene lists using DAVID bioinformatics resources. Nat Protoc. 2009;4(1):44–57.

1121 52. Shepherd TM, Flint JJ, Thelwall PE, Stanisz GJ, Mareci TH, Yachnis AT, et al.
1122 Postmortem interval alters the water relaxation and diffusion properties of rat
1123 nervous tissue--implications for MRI studies of human autopsy samples. NeuroImage.
1124 2009 Feb 1;44(3):820–6.

1125 53. Cotter DR, Pariante CM, Everall IP. Glial cell abnormalities in major psychiatric
1126 disorders: The evidence and implications. Brain Res Bull. 2001 Jul 15;55(5):585–95.

1127 54. Banasr M, Duman RS. Glial loss in the prefrontal cortex is sufficient to induce
1128 depressive-like behaviors. Biol Psychiatry. 2008 Nov 15;64(10):863–70.

1129 55. Guidotti A, Auta J, Davis JM, Di-Giorgi-Gerevini V, Dwivedi Y, Grayson DR, et al.
1130 Decrease in reelin and glutamic acid decarboxylase67 (GAD67) expression in
1131 schizophrenia and bipolar disorder: a postmortem brain study. Arch Gen Psychiatry.
1132 2000 Nov;57(11):1061–9.

1133 56. Hashimoto T, Volk DW, Eggan SM, Mirnics K, Pierri JN, Sun Z, et al. Gene expression
1134 deficits in a subclass of GABA neurons in the prefrontal cortex of subjects with
1135 schizophrenia. J Neurosci Off J Soc Neurosci. 2003 Jul 16;23(15):6315–26.

1136 57. Volk DW, Austin MC, Pierri JN, Sampson AR, Lewis DA. Decreased glutamic acid
1137 decarboxylase67 messenger RNA expression in a subset of prefrontal cortical gamma-
1138 aminobutyric acid neurons in subjects with schizophrenia. Arch Gen Psychiatry. 2000
1139 Mar;57(3):237–45.

1140 58. Morris HM, Hashimoto T, Lewis DA. Alterations in somatostatin mRNA expression in
1141 the dorsolateral prefrontal cortex of subjects with schizophrenia or schizoaffective
1142 disorder. Cereb Cortex N Y N 1991. 2008 Jul;18(7):1575–87.

1143 59. Volk D, Austin M, Pierri J, Sampson A, Lewis D. GABA transporter-1 mRNA in the
1144 prefrontal cortex in schizophrenia: decreased expression in a subset of neurons. Am J
1145 Psychiatry. 2001 Feb;158(2):256–65.

1146 60. Glantz LA, Lewis DA. Reduction of synaptophysin immunoreactivity in the prefrontal
1147 cortex of subjects with schizophrenia. Regional and diagnostic specificity. Arch Gen
1148 Psychiatry. 1997 Jul;54(7):660–9.

1149 61. Pandey GN, Dwivedi Y, Rizavi HS, Ren X, Pandey SC, Pesold C, et al. Higher expression
1150 of serotonin 5-HT(2A) receptors in the postmortem brains of teenage suicide victims.
1151 Am J Psychiatry. 2002 Mar;159(3):419–29.

1152 62. Bu J, Sathyendra V, Nagykery N, Geula C. Age-related changes in calbindin-D28k,
1153 calretinin, and parvalbumin-immunoreactive neurons in the human cerebral cortex.
1154 Exp Neurol. 2003 Jul;182(1):220–31.

1155 63. Girgenti MJ, LoTurco JJ, Maher BJ. ZNF804a regulates expression of the schizophrenia-
1156 associated genes PRSS16, COMT, PDE4B, and DRD2. PloS One. 2012;7(2):e32404.

1157 64. Le-Niculescu H, Patel SD, Bhat M, Kuczenski R, Faraone SV, Tsuang MT, et al.
1158 Convergent functional genomics of genome-wide association data for bipolar disorder:
1159 comprehensive identification of candidate genes, pathways and mechanisms. Am J
1160 Med Genet Part B Neuropsychiatr Genet Off Publ Int Soc Psychiatr Genet. 2009 Mar
1161 5;150B(2):155–81.

1162 65. Choi KH, Higgs BW, Wendland JR, Song J, McMahon FJ, Webster MJ. Gene expression
1163 and genetic variation data implicate PCLO in bipolar disorder. Biol Psychiatry. 2011
1164 Feb 15;69(4):353–9.

1165 66. Mistry M, Gillis J, Pavlidis P. Genome-wide expression profiling of schizophrenia using
1166 a large combined cohort. Mol Psychiatry. 2013 Feb;18(2):215–25.

1167 67. Hyde CL, Nagle MW, Tian C, Chen X, Paciga SA, Wendland JR, et al. Identification of 15
1168 genetic loci associated with risk of major depression in individuals of European
1169 descent. Nat Genet. 2016 Sep;48(9):1031–6.

1170 68. Rao JS, Harry GJ, Rapoport SI, Kim HW. Increased excitotoxicity and
1171 neuroinflammatory markers in postmortem frontal cortex from bipolar disorder
1172 patients. Mol Psychiatry. 2010 Apr;15(4):384–92.

1173 69. Spiliotaki M, Salpeas V, Malitas P, Alevizos V, Moutsatsou P. Altered glucocorticoid
1174 receptor signaling cascade in lymphocytes of bipolar disorder patients.
1175 Psychoneuroendocrinology. 2006 Jul;31(6):748–60.

1176 70. Konopaske GT, Subburaju S, Coyle JT, Benes FM. Altered prefrontal cortical MARCKS
1177 and PPP1R9A mRNA expression in schizophrenia and bipolar disorder. Schizophr Res.
1178 2015 May;164(1–3):100–8.

1179 71. Glessner JT, Reilly MP, Kim CE, Takahashi N, Albano A, Hou C, et al. Strong synaptic
1180 transmission impact by copy number variations in schizophrenia. Proc Natl Acad Sci U
1181 S A. 2010 Jun 8;107(23):10584–9.

1182 72. Ayoub MA, Angelicheva D, Vile D, Chandler D, Morar B, Cavanaugh JA, et al. Deleterious
1183 GRM1 mutations in schizophrenia. PloS One. 2012;7(3):e32849.

1184 73. Frank RAW, McRae AF, Pocklington AJ, van de Lagemaat LN, Navarro P, Croning MDR,
1185 et al. Clustered coding variants in the glutamate receptor complexes of individuals
1186 with schizophrenia and bipolar disorder. PloS One. 2011;6(4):e19011.

1187 74. Chase KA, Rosen C, Gin H, Bjorkquist O, Feiner B, Marvin R, et al. Metabolic and
1188 inflammatory genes in schizophrenia. Psychiatry Res. 2015 Jan 30;225(1–2):208–11.

1189 75. Etain B, Dumaine A, Mathieu F, Chevalier F, Henry C, Kahn J-P, et al. A SNAP25
1190 promoter variant is associated with early-onset bipolar disorder and a high
1191 expression level in brain. Mol Psychiatry. 2010 Jul;15(7):748–55.

1192 76. Fatjó-Vilas M, Prats C, Pomarol-Clotet E, Lázaro L, Moreno C, González-Ortega I, et al.
1193 Involvement of NRN1 gene in schizophrenia-spectrum and bipolar disorders and its
1194 impact on age at onset and cognitive functioning. World J Biol Psychiatry Off J World
1195 Fed Soc Biol Psychiatry. 2016;17(2):129–39.

1196 77. Volk DW, Chitrapu A, Edelson JR, Roman KM, Moroco AE, Lewis DA. Molecular
1197 mechanisms and timing of cortical immune activation in schizophrenia. Am J
1198 Psychiatry. 2015 Nov 1;172(11):1112–21.

1199 78. Tasic B, Menon V, Nguyen TN, Kim TK, Jarsky T, Yao Z, et al. Adult mouse cortical cell
1200 taxonomy revealed by single cell transcriptomics. Nat Neurosci. 2016 Feb;19(2):335–
1201 46.

1202 79. Mancarci O, Toker L, Tripathy S, Li B, Rocco B, Sibille E, et al. NeuroExpresso: A cross-
1203 laboratory database of brain cell-type expression profiles with applications to marker
1204 gene identification and bulk brain tissue transcriptome interpretation. bioRxiv
1205 [Internet]. 2016 Nov 22; Available from:
1206 http://biorxiv.org/content/biorxiv/early/2016/11/22/089219.full.pdf

1207 80. Oldham MC, Konopka G, Iwamoto K, Langfelder P, Kato T, Horvath S, et al. Functional
1208 organization of the transcriptome in human brain. Nat Neurosci. 2008
1209 Nov;11(11):1271–82.

1210 81. Cheadle C, Cho-Chung YS, Becker KG, Vawter MP. Application of z-score
1211 transformation to Affymetrix data. Appl Bioinformatics. 2003;2(4):209–17.

1212 82. Montaño CM, Irizarry RA, Kaufmann WE, Talbot K, Gur RE, Feinberg AP, et al.
1213 Measuring cell-type specific differential methylation in human brain tissue. Genome
1214 Biol. 2013;14(8):R94.

1215 83. Atz M, Walsh D, Cartagena P, Li J, Evans S, Choudary P, et al. Methodological
1216 considerations for gene expression profiling of human brain. J Neurosci Methods.
1217 2007 Jul 30;163(2):295–309.

1218 84. Vawter MP, Tomita H, Meng F, Bolstad B, Li J, Evans S, et al. Mitochondrial-related gene
1219 expression changes are sensitive to agonal-pH state: implications for brain disorders.
1220 Mol Psychiatry. 2006 Jul;11(7):615, 663–79.

1221 85. Li JZ, Bunney BG, Meng F, Hagenauer MH, Walsh DM, Vawter MP, et al. Circadian
1222 patterns of gene expression in the human brain and disruption in major depressive
1223 disorder. Proc Natl Acad Sci U S A. 2013 Jun 11;110(24):9950–5.

1224 86. Hamberger A, Hyden H. Inverse enzymatic changes in neurons and glia during
1225 increased function and hypoxia. J Cell Biol. 1963 Mar;16:521–5.

1226 87. Bowling K, Ramaker RC, Lasseigne BN, Hagenauer M, Hardigan A, Davis N, et al. Post-
1227 mortem molecular profiling of three psychiatric disorders reveals widespread
1228 dysregulation of cell-type associated transcripts and refined disease-related
1229 transcription changes. bioRxiv. 2016 Jun 29;061416.

88. Medina A, Watson SJ, Bunney W, Myers RM, Schatzberg A, Barchas J, et al. Evidence for alterations of the glial syncytial function in major depressive disorder. J Psychiatr Res. 2016 Jan;72:15–21.

89. Turner CA, Watson SJ, Akil H. The fibroblast growth factor family: neuromodulation of affective behavior. Neuron. 2012 Oct 4;76(1):160–74.

90. American Psychiatric Association. Diagnostic and Statistical Manual of Mental Disorders (DSM-IV-TR). 4th ed. Washington, D.C.: American Psychiatric Association; 2000.

91. Dai M, Wang P, Boyd AD, Kostov G, Athey B, Jones EG, et al. Evolving gene/transcript definitions significantly alter the interpretation of GeneChip data. Nucleic Acids Res. 2005;33(20):e175.

92. Irizarry RA, Hobbs B, Collin F, Beazer-Barclay YD, Antonellis KJ, Scherf U, et al. Exploration, normalization, and summaries of high density oligonucleotide array probe level data. Biostat Oxf Engl. 2003 Apr;4(2):249–64.

93. Allen Brain Atlas. Technical White Paper: Microarray Data Normalization, v.1 [Internet]. 2013. Available from: help.brain-map.org

7. Supporting Information Captions

S1 Text. Supplementary Methods & Results

S2 Text. Supplementary Figures and Figure Legends.

S1 Table. Master Database of Cortical Cell Type Specific Gene Expression. The attached excel document contains a single spreadsheet listing the genes defined as having cell type specific expression in our manuscript, including the species, age of the subjects, and brain region from which the cells were purified, the platform used to measure transcript, the statistical criteria and comparison cell types used to define "cell type specific expression", the gene symbol or orthologous gene symbol in mouse/human (depending on the species used in the original experiment), and citation. If a gene was identified as having cell type specific expression in multiple experiments, there is an entry for each experiment – thus the full 3383 rows included in the spreadsheet do not represent 3383 individual cell type specific genes. A web-version of this spreadsheet kept interactively up-to-date can be found at https://sites.google.com/a/umich.edu/megan-hastings-hagenauer/home/cell-type-analysis.

S2 Table. Sample demographics for the Pritzker Consortium Dorsolateral Prefrontal Cortex Affymetrix microarray data.

S3 Table. Microarray data spanning 160 human brain regions downloaded from the Allen Brain Atlas. Included in this excel file are three worksheets. The first includes all of the sample information, including the subject identifier and brain region. The second includes all of the probe information. Finally, the third includes the relative expression for each probe for each sample (z-score), including the official gene symbol, Entrez gene ID, and gene name. Additional information about the human microarray dataset can be found on the Allen Brain Atlas website.

S4 Table. The relationship between each cell type index and all probes in the Pritzker Dorsolateral Prefrontal Cortex dataset. The attached excel document (.xlsx) contains multiple spreadsheets. The first spreadsheet ("Methods") contains a brief summary of the methods used to evaluate the relationship between the cell type indices and expression of each probe in the dataset (also discussed in the body of the manuscript). The second spreadsheet ("GeneByCellType_DF") contains the statistical output associated with all cell type index terms in the linear model for all probes in the dataset, including the β ("Beta": magnitude and direction of the association, with positive associations labeled pink and negative associations labeled blue), the p-value from the original model ("Pval") and the p-value adjusted for multiple comparisons using the Benjamini-Hochberg method ("AdjP"), both labeled with green indicating more significant relationships and red indicating less significant relationships. All other spreadsheets contain the top 100 probes positively associated with each cell type index, including each of the statistical outputs presented in the full "GeneByCellType_DF"

1294 summary spreadsheet, as well as a column “CellTypeSpecific” which indicates whether
1295 the probe was included in one of the original cell type indices (1=included, 0=not
1296 included).
1297
1298 **S5 Table. The average cell type indices for all 160 brain regions included in the**
1299 **Allen Brain Atlas dataset.** This excel file contains two worksheets. The first includes
1300 the average cell type index for 10 primary cell types for all 160 brain regions included in
1301 the Allen Brain Atlas. More detail about those brain regions can be found in the first
1302 worksheet (Columns_Sample Info) in **Supplementary Table 3**. The second
1303 spreadsheet contains the standard error (SE) for the averages in the first worksheet.
1304
1305 **S6 Table. The relationship between each cell type index and all probes in the**
1306 **Allen Brain Atlas dataset.** Depicted are the β (magnitude and direction) and p-values
1307 for the relationship between the expression for each probe and each primary cell type
1308 across samples from all 160 brain regions as determined in a large linear model that
1309 includes all 10 primary cell types. Please note that the p-values in this spreadsheet
1310 have not been corrected for multiple comparisons. Additional information about the
1311 probes can be found in **Supplementary Table 3**.
1312
1313 **S7 Table. Functions associated with genes identified as having neuron-specific**
1314 **expression.** The first column of the excel spreadsheet is a list of general physiological
1315 functions that were identified by DAVID as associated with our list of neuron-specific
1316 genes (relative to the full list of probesets included in the microarray). We used the

1317 functional cluster option in DAVID because it prevents multiple functions that share a
1318 large subset of overlapping genes from dominating the results. We named each cluster
1319 by the top two functions included in it. The second column of the spreadsheet indicates
1320 whether an experimenter blindly categorized the functional cluster as being clearly
1321 related or unrelated to synaptic function. The "Mean Fold Enrichment" column indicates
1322 how well on average each of the functions within that cluster were associated with our
1323 list of neuron-specific genes. The next three columns (Top p-value, Top Bonferronni-
1324 corrected p-value, and top BH (Benjamini-Hochberg)-corrected p-value) indicate the
1325 statistical strength of the association between the top function within that cluster and our
1326 list of neuron-specific genes. The number of genes from each functional cluster included
1327 in our results is listed in column G. The next few columns indicate the strength of the
1328 relationship between the functional cluster and age. Columns H-J indicate the mean,
1329 standard deviation, and standard error, for the betas for Age for each gene included in
1330 the cluster. The betas indicate the strength and direction of the association with Age as
1331 determined within a larger linear model controlling for known confounds (pH, PMI,
1332 gender, agonal factor). Columns K-M indicate whether, on average, the age-related
1333 betas for the genes in that cluster are statistically different from 0 as determined by a
1334 Welch's t-test (t-stat, df, p-value). The final column indicates what percentage of the
1335 genes included in the cluster have a negative relationship (β) with age.
1336

1337 **S8 Table. The relationship between diagnosis and all probes in the Pritzker**
1338 **Dorsolateral Prefrontal Cortex dataset using a traditional model that controls for**
1339 **standard confounds (*Equation 3* in Figure 5).** For all probes in the dataset, the

spreadsheet includes the β ("Beta": magnitude and direction of the association, with positive associations labeled pink and negative associations labeled blue), the p-value from the original model ("Pval_nominal") and the p-value adjusted for multiple comparisons using the Benjamini-Hochberg method ("BH_Adj"), both labeled with green indicating more significant relationships and red indicating less significant relationships.

S9 Table. The relationship between psychiatric illness and all probes in the Pritzker Dorsolateral Prefrontal Cortex dataset using a traditional model that controls for standard confounds (*Equation 3* in Figure 5). For all probes in the dataset, the spreadsheet includes the β ("Beta": magnitude and direction of the association, with positive associations labeled pink and negative associations labeled blue), the p-value from the original model ("Pval_nominal") and the p-value adjusted for multiple comparisons using the Benjamini-Hochberg method ("BH_Adj"), both labeled with green indicating more significant relationships and red indicating less significant relationships.

S10 Table. The relationship between diagnosis and all probes in the Pritzker Dorsolateral Prefrontal Cortex dataset using a model that controls for standard confounds and the five most prevalent cortical cell types (*Equation 6* in Figure 5). For all probes in the dataset, the spreadsheet includes the β ("Beta": magnitude and direction of the association, with positive associations labeled pink and negative associations labeled blue), the p-value from the original model ("Pval_nominal") and the p-value adjusted for multiple comparisons using the Benjamini-Hochberg method

("BH_Adj"), both labeled with green indicating more significant relationships and red indicating less significant relationships.

S11 Table. The relationship between psychiatric illness and all probes in the Pritzker Dorsolateral Prefrontal Cortex dataset using a model that controls for standard confounds and the five most prevalent cortical cell types (*Equation 6* in Figure 5). For all probes in the dataset, the spreadsheet includes the β ("Beta": magnitude and direction of the association, with positive associations labeled pink and negative associations labeled blue), the p-value from the original model ("Pval_nominal") and the p-value adjusted for multiple comparisons using the Benjamini-Hochberg method ("BH_Adj"), both labeled with green indicating more significant relationships and red indicating less significant relationships.